Part II
Biomarker and Molecular Probes

Chapter 6
How Far Are We from Dose On Demand of Short-Lived Radiopharmaceuticals?

Giancarlo Pascali and Lidia Matesic

Abstract PET radiopharmaceuticals are currently produced using a centralized approach, which makes sustainable the distribution to few imaging centers of an only small set of tracers (virtually only [^{18}F]FDG). However, a wider set of structures have demonstrated a potential applicability for imaging in a specific manner several disease condition. In order to allow this wider and more personalized use of PET imaging, the production paradigms need to be changed. In this contribution we will explain how Dose-On-Demand systems can be conceptualized and what are the challenges that are still to be overcome in order for such approach to be of widespread utility.

Keywords Dose On Demand • Microfluidics • PET • Radiochemistry

6.1 Introduction

The clinical production of radiopharmaceuticals or radiotracers for positron-emitting tomography (PET) is currently performed in centralized locations such as commercial radiopharmacies or some dedicated radiochemistry facilities. Generally, these facilities contain a cyclotron to produce the PET radioisotope and laboratories furnished with lead-shielded hot cells containing automated radiosynthesis modules to produce the radiotracer. Quality control equipment is also required to validate and confirm the purity of the radiotracer prior to its dispatch to the imaging centers.

The majority of radiotracer production facilities synthesize [^{18}F]FDG, the gold standard for detecting a variety of cancers. Nowadays, [^{18}F]FDG can be produced in a large batch, making it relatively affordable. Portions can then be dispatched and transported by road or air to the relevant hospital owing to the half-life of fluorine-18 (110 min).

G. Pascali (✉) • L. Matesic
ANSTO LifeSciences, Cyclotron building 81, Missenden Rd, Camperdown, NSW 2050, Australia
e-mail: gianp@ansto.gov.au

Y. Kuge et al. (eds.), *Perspectives on Nuclear Medicine for Molecular Diagnosis and Integrated Therapy*, DOI 10.1007/978-4-431-55894-1_6

A major challenge in clinical PET radiochemistry is that there are a greater number of hospitals or PET clinics than there are PET radiotracer production facilities. Furthermore, the demand for new clinical PET radiotracers is low due to the cost of production in a centralized location. New PET radiotracers are overwhelmingly used for research purposes only.

To overcome this obstacle, a decentralized approach has been envisaged [1]. Here, scientists could produce their radiotracer of interest in-house, economically and on demand, leading to a concept that we have defined as Dose On Demand (DOD). This short review will cover the important aspects of DOD and detail the journey toward the DOD of short-lived radiopharmaceuticals.

6.2 DOD Features

The current production approach of PET radiotracers imposes several limitations and challenges for guaranteeing the most efficient organization of imaging studies [2]. A possible way to improve this situation would require a system for which the type and the quantity of the produced tracer is defined and directly handled by an as final as possible user (e.g., hospital pharmacy, imaging laboratory). This system should implement the reduction to the minimum possible of the amounts of radioactivity and chemicals needed in the preparation, added to an overall simplification of the production process. Such conceptual process can be defined as "Dose On Demand" (*DOD*) [3, 4, 5]: the operation of producing a radiopharmaceutical in the shortest time possible, using the minimum amount of chemicals and radioactivity strictly needed for the production of the single (or few) imaging dose (s) required.

This approach, exemplified in Fig. 6.1, would provide several benefits to the overall PET community. Firstly, it will hand over *flexibility* in the application directly to the hospital/imaging center, which can decide on a patient basis which tracer to produce and when; this could also happen in small regional centers, thus not forcing anymore interested patients to commute long distances to the few useful imaging hospitals. This flexibility will also allow the utilization of rare or research tracers to be facilitated, as in this system the small amounts of chemicals and radioactivity needed for a DOD production would be economically sustainable for a single imaging center. Secondly, while a fault in production from a centralized approach will have impact on a large number of patients, a *fault* in one DOD system will have an impact limited to the patients utilizing those doses only. Lastly, due to the *reduction* in raw materials needed (as well as related topics, e.g., safety, storage) and the redistribution of running costs over more institutes, the imaging doses will result in a reduced cost and in tracers' availability to a wider population.

In order to realize a DOD process, few requirements can be envisaged.

Firstly, the production needs to be implemented on an automated instrument that can implement preset operations, as well as allowing remote interaction of the operator for minor modifications (i.e., "Automation"). In addition, it has to have

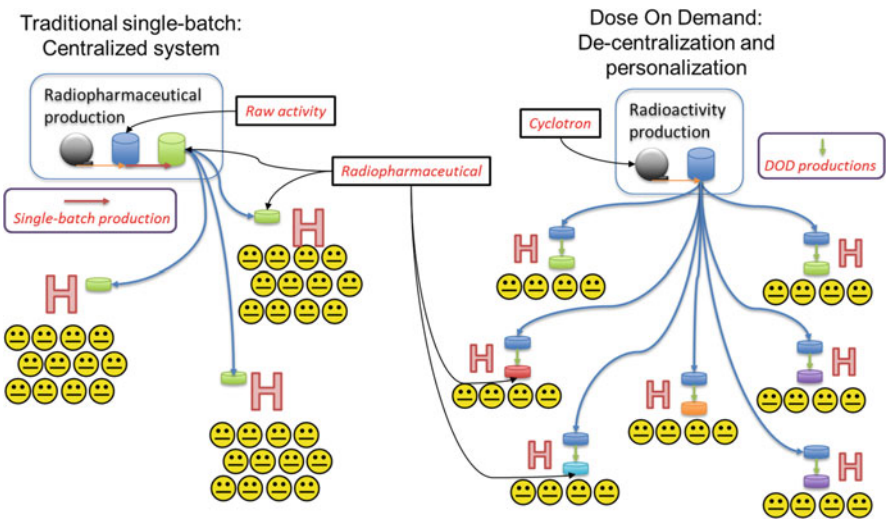

Fig. 6.1 Comparison between traditional centralized approach and DOD

real-time monitoring and audit trail capabilities for monitoring and trending purposes. Secondly, the instrument used needs to be able to handle small aliquots of reagents, from fractions to hundreds of μL (i.e., "Discretization") with accuracy and repeatability. The handling operations comprise moving, merging, mixing, heating, and similar processes. In other words, the instrument has to be capable to give a defined "chemical history" to any given aliquot of reagents used (that can be different among several aliquots). Thirdly, the processes implemented need to be serially repeatable with minimum operator intervention ("Restarting"). This can be achieved by substituting single-use parts in the system or by cleaning it using validated procedures. A final peculiarity that contributes to achieving DOD is the need to use the minimum amount of chemicals ("Reduction"), which would maximize the atom efficiency of the process, as well as allow an acceptable sacrifice in employing single-use parts or realize a faster cleaning of the system.

If all these requirements can be respected in a process system, a DOD production can be implemented and can be used to produce several doses of the same tracer or of different tracers, using the same system and minimal operator interventions.

6.3 Early Examples Conducible to DOD

The possibility to tailor the production of nuclear medicine (NM) tracers as much as possible to the needs of the final user has always been present, and indeed some example of approaches that can be linked to DOD concept can be found in early and current practices.

Generators of radioactive raw nuclides have been widely used (e.g., ^{99m}Tc, ^{68}Ga) [6]; the elution of the desired radionuclide is generally done upon demand and followed by simple chemical reactions (generally performed directly in the same NM department) to obtain the final radiopharmaceutical. This approach respects the Restarting requirement, though limited to the raw nuclide production and not to the pharmaceutical preparation; however, it generally does not respect the Discretization nor the Reduction requirements, as it is difficult to separately handle the amount of chemicals needed for a single patient (i.e., in the μLs range). It sometimes respects the Automation requirement, but in most NM departments, these preparations are performed manually.

The use of very *short half-life* nuclides can be natively defined as a DOD application, as their handling must be done shortly before their use in imaging. Typical examples are the production of [^{15}O]-H_2O [7] and [^{13}N]-NH_3 [8]; shortly after production, the systems utilized can be restarted easily due to their simple setup and the fast decay of process wastes. However, also in this case, these processes cannot be properly defined as DOD since they generally respect the Automation and the Restarting requirements, but neither the Discretization nor the Reduction (i.e., no difference if the production is used for one or several contemporary patients). ^{11}C chemistry [8] also falls within the use of very short half-life nuclides as more productions can be run on the same machine on the same day. However, also in this case, the typical systems used can be even less defined as DOD, due to its relatively longer half-life (compared to ^{15}O and ^{13}N).

Currently, the approach that most resembles DOD is represented by the *cassette-based* systems. In this case, Automation and Restarting requirements can be easily achieved; Discretization and Reduction are generally not pursued, because nowadays these systems are used for single-batch productions, but the principles underlying cassette philosophy could be used to project single-use/single-dose cassettes. In fact, these systems are basically very compact macrofluidic systems; this understanding clarifies how *microfluidic* concepts can be the ones that should allow a full implementation of DOD in radiopharmaceutical production.

6.4 DOD Proof-of-Principle Examples

6.4.1 Minicyclotron/Minichemistry/MiniQC

The Biomarker Generator (BG75), made by ABT Molecular Imaging, is a small (0.37 m × 1.25 m) self-shielded 7.5 MeV cyclotron coupled to an aseptic single-use card-based automated chemical production module and an automated module for quality control. The BG75 was initially used for the DOD production of [^{18}F] fluoride and [^{18}F]FDG [9]. Using the computer's software, the operator is able to select whether the [^{18}F]fluoride or [^{18}F]FDG is to be produced. For the production of [^{18}F]fluoride (~1 mCi/min at 5 μA), the process is complete once the product is delivered into the specified vial. Alternatively, for the production of [^{18}F]FDG, the

software prompts the operator to prepare the tracer-specific Dose Synthesis Card (DSC) and the chemistry and quality control modules while the cyclotron is preparing the [^{18}F]fluoride. The radiosynthesis is then completed on the DSC, including relevant purification, and dispensed into a shielded, sterile syringe or vial. An aliquot of the product is removed for quality control (pH determination, acetonitrile and ethanol residual solvent determination, radiochemical identity and purity, Kryptofix 2.2.2. determination, and a filter integrity test), which is automatically performed by the system, without any operator input.

The BG75 has been able to consistently produce a 10–13 mCi dose of [^{18}F]FDG at 40 min intervals up to six times per day, with products meeting the required USP limits for release [9]. To date, other DOD radiotracers synthesized using the BG75 include Na[^{18}F]F [10] and [^{18}F]FMISO [11, 12].

6.4.2 Continuous Flow Microfluidics

Interestingly, proof-of-concept studies have been recently conducted into the production of [^{18}F]FLT using the cyclotron component of the BG75 system and the Advion NanoTek microfluidic system [13]. Between 70 and 80 mCi of [^{18}F]fluoride were produced by the minicyclotron and the radiosynthesis was subsequently performed under continuous-flow microfluidic conditions to yield [^{18}F]FLT in sufficient quantity and purity for clinical trials. The number of radiochemists using a microfluidic approach has been steadily accumulating in recent years. This may be related to the advantages of microfluidic systems over traditional automated radiochemistry modules, which include a decrease in the amount chemical reagents used, shorter reaction times, greater radiochemical yields, the ability to use solvents under supercritical conditions, and reduced radiation exposure to the operator due to the lower amounts of radioactivity used. The NanoTek Microfluidic Synthesis System by Advion was the first commercially available continuous-flow microfluidic system. The system comprises a concentrator module to azeotropically evaporate the [^{18}F]fluoride from the cyclotron and subsequently reconstitute the isotope into the appropriate solvent; a pump module containing two syringe pumps and loops to store chemical precursors and a reactor module, which contains a syringe pump and loop to house the isotope along with thermostatted slots to store up to four microreactors, where the radiochemical reactions occur.

The previous example of the production of [^{18}F]FLT is the latest in a growing list of radiotracers prepared using the NanoTek system. The first instance was the production of [^{18}F]fallypride for use in micro-PET studies [14]. Initially, the radiochemical optimization of [^{18}F]fallypride was conducted by dispensing 10 μL solutions of the tosyl-fallypride precursor and [^{18}F]fluoride complex into the microreactor at 10 μL/min to obtain 1–1.5 mCi doses of [^{18}F]fallypride. These optimization reactions were performed sequentially and could be considered an early form of DOD. Once the optimal radiochemical conditions were determined, the authors were able to prepare a dose of [^{18}F]fallypride sufficient for human injection (15 mCi) by increasing the volume of the two solutions from 10 μL to

200 μL. The authors also alluded to the fact that multiple high doses of [^{18}F] fallypride could be produced using the same microreactor. Soon after, Pascali et al. [15] described the sequential radiolabeling of ethyl-ditosylate and propyl-ditosylate in the NanoTek system using the same solution of [^{18}F]fluoride complex and swapping the precursor between productions by emptying and refilling the precursor loop with a different substrate. These examples of DOD demonstrated the economical use of the [^{18}F]fluoride solution to yield two radiotracers on the same day. The authors also sequentially prepared several injectable doses of [^{18}F]CB102, a cannabinoid type 2 receptor agonist, for small animal PET imaging, suggesting that freshly prepared doses using a DOD approach were superior to a batch solution to be used over a certain shelf life.

To further evaluate the robustness and reliability of a DOD approach, Pascali et al. were able to produce three sequential doses of three different [^{18}F] fluorocholines with a total processing time of 13–15 min for each dose, including SPE purification [5]. While this example includes a modification to the NanoTek system to incorporate SPE purification, typically, the radiochemical outputs are purified externally to the NanoTek system, particularly HPLC purification. Recent examples include the preparation of [^{18}F]FPEB [16], whereby the radiosynthesis occurred in the NanoTek and the reaction output was sent to a vial preloaded with water and pre-concentrated onto an Oasis HLB Light SPE cartridge to remove DMSO present in the reaction mixture. The cartridge was eluted with acetonitrile and water before being transferred to a GE TRACERlab F_XF_N synthesis unit to conduct semi-preparative HPLC purification and formulation. Additionally, the Tau imaging agent, [^{18}F]T807, was produced with the same modifications [17]. Three consecutive >100 mCi productions of [^{18}F]T807 were performed for validation purposes, and [^{18}F]T807 became the first example of human use of a radiopharmaceutical prepared by continuous-flow microfluidics.

The NanoTek system has been modified recently to include HPLC and SPE purification [18]. By utilizing the cable harnessing of the system, a custom-made electrical board was engineered whereby additional switches and analog signals could be added and be controlled by the NanoTek software to activate externally powered devices and record external signals (e.g., detectors), if applicable. This customized system was able to produce 1- or 2-step radiotracers such as [^{18}F] CB102, [^{18}F]fluoroethylcholine [18], [^{18}F]MEL050 (melanin targeting) [19], [^{18}F] fallypride, and [^{18}F]PBR111 (TSPO receptor) [20], in a DOD manner. Similarly, [^{18}F]FMISO has been produced by integrating a HPLC system to the NanoTek through a six-port valve [21]. By fine-tuning the HPLC conditions for [^{18}F]FMISO, the authors were able to eliminate the requirement for SPE.

6.4.3 Peptide Labeling

While microfluidic systems have mainly been utilized to radiolabel small molecules, reports of peptide or protein radiolabeling using microfluidics are limited.

Early work in this area featured the direct [^{18}F]radiolabeling of bombesin derivatives (with 7–8 amino acid residues) that had been modified to incorporate trimethylammonium or triarylsulfonium leaving groups [22]. The peptides could be radiolabeled reproducibly, suggesting a possible DOD approach; however, due to the harsh temperature conditions required for radiolabeling, this method would be unsuitable for protein radiolabeling. An alternative route to radiolabel a peptide is through the use of a prosthetic group as an indirect radiolabeling method. [^{18}F]SFB [23] and even, the most abundantly used PET tracer, [^{18}F]FDG [24] have been utilized as prosthetic groups for the radiolabeling of peptides. Although both prosthetic groups were synthesized on macroscale equipment, the subsequent peptide radiolabeling was performed under microfluidic conditions. In each case, the peptide was radiolabeled in a shorter period of time, in higher radiochemical yield (RCY), and using a smaller quantity of the peptide compared to conventional radiolabeling techniques. Only recently has the first microfluidic radiosynthesis of a prosthetic group and the ensuing peptide radiolabeling been reported [25]. Here, the [^{18}F]F-Py-TEP prosthetic group was prepared in the first microreactor of an Advion NanoTek system from [^{18}F]fluoride and the corresponding precursor. After exiting the microreactor, the [^{18}F]F-Py-TEP was transferred to a second microreactor, where it reacted with a model peptide containing free amines. Once again, the peptide coupling was faster than conventional methods and obtained in higher RCY. These accounts all imply that the DOD of radiolabeled peptides for molecular imaging is currently being explored and may be employed in the future.

6.4.4 Solid-Phase Approaches

Although the use of microfluidic conditions is leading to radiochemical reactions being completed in less time than traditional approaches, to further decrease the overall radiochemical processing times, new methods are required to decrease or eliminate the time taken to process and activate the starting [^{18}F]fluoride. One option is to trap the [^{18}F]fluoride onto a resin and subsequently perform on-resin radiofluorinations, thus eliminating the need for azeotropic evaporations and re-solubilization of the [^{18}F]fluoride complex. Reusable polymer-supported phosphazenes have been investigated as suitable resins to perform the [^{18}F]fluoride trapping and radiofluorination [26]. The PS-P_2^{tBu} resin was able to trap >99% of [^{18}F]fluoride, with no leaching of activity was observed when the column was subsequently dried with helium gas. It was found that substrates with sulfonate leaving groups resulted in the highest RCY when subjected to on-column radiofluorination. The same phosphazene resin could be recycled at least three times using the same substrate, or at least two times using a different substrate, which implies that the DOD production of radiotracers is possible through solid-phase radiofluorination.

Other work in this area includes a continuous-flow system comprising a polystyrene-imidazolium-chloride (PS-Im$^+$Cl$^-$) monolith which traps [^{18}F]fluoride [27]. A solution of base and the relevant precursor could then be flowed through the

PS-Im$^+$[^{18}F]F$^-$ monolith into a preheated microfluidic chip where the radiochemical reaction takes place. The advantage of this method is that the entire process is performed in continuous flow and the microfluidic platform has a very small footprint compared to current processes.

6.4.5 Droplet Systems

An interesting extension in the field of microfluidic radiochemistry is through the use of droplets. Also sometimes referred to as segmented flow chemistry, it features droplets (nL- μL) which are separated by an immiscible carrier fluid, similar to oil droplets in water. Droplets can be thought of as individual nano- or microreactors and can be used to aid radiolabeling optimization, whereby each droplet is the result of a predetermined set of reaction parameters. Droplets consisting of approximately 120 nL were formed during the coupling of [^{18}F]FSB with an anti-prostate stem cell antigen diabody [28]. Using a 5 μL sample of the diabody solution was sufficient to screen over 100 different reaction conditions using the droplets, and hence, the optimal reaction conditions were determined rapidly with minimal use of the precious diabody solution. Droplet systems have also been utilized in electrowetting-on-dielectric (EWOD) devices. In EWOD systems, droplets are sandwiched between two plates; the bottom plate consists of electrode pads to manipulate the movement of the droplets throughout the microchip, while the top plate electrically grounds the droplets. The EWOD chip was first used in the synthesis of [^{18}F]FDG [29], but its use has more recently expanded to include [^{18}F]FLT [30], [^{18}F]fallypride [31], and [^{18}F]SFB [32]. While the EWOD chip produces these radiolabeled molecules in comparable, if not greater, RCY than previously, drawbacks of the system include off-chip purification and the potential for radioactivity and volatile side products to escape since the chip is exposed to air. It is envisaged that with advances in technology, the EWOD chip could be further automated, be disposable, and lead to scientists producing their desired radiotracer on demand.

6.5 Challenges and Future of DOD

As it can be seen, a perfect DOD system is still not existent, but several data are available demonstrating that such approach should represent the reality in the next future. However, to witness this paradigmatic change, several challenges need to be fronted, and they will represent the future of DOD research in radiopharmaceutical production.

One of the biggest challenges is to understand whether one only system could achieve the desired spread of operations that a DOD process should implement. This should cover not only the production steps but also the switching of chemicals, cleaning, and priming steps. It is very likely that these systems will be based on

micronized approaches (e.g., microfluidics, nanodroplets), but understanding which *philosophy* they should implement is still under discussion. For example, a system can be projected to implement several different preexisting routes, which would lead to different products in different quantities, or, on the contrary, be represented by a fixed framing to which flexibly interface single-use components/modules (i.e., similar to microcassettes) to build up the desired process. Another possibility might also be represented by the possibility to use the exact same system into which different chemicals are delivered, depending on the production needs. All these options are amenable to deliver a DOD system, but the choice of one or the other will drive the final performance and actual ease/flexibility of use.

Even once the underlying philosophy is clarified, some technical problems are still unsolved or partially addressed. *Purification* of the finished product represents probably the most important issue, and while there are several excellent systems to perform chemical reactions, there is a notable lack in miniaturization of purification methods or their interfacing with micronized chemistry systems. Some research is now available on micro-chromatographic systems [33], mainly facilitated by the advancements of monolith polymers [34] that can be easily integrated with micron-sized channels/reservoirs [35]. These solutions allow the reduction of inherent void volumes, therefore improving the atom efficiency in the purification process. Also, similar solutions may be useful for the cases in which a simple solid-phase extraction (SPE) would be sufficient to purify the relevant molecule [36, 37]. Polymer chemistry advancement possibly represents the field where useful innovations can have a relevant impact on miniaturized purifications. As an example, molecularly imprinted polymers (MIP) represent a promising approach that would allow to streamline the selective separation of the molecule of interest and its efficient elution [38]. MIP structures are prepared by building the polymer pores around a desired template molecule; once the template is removed, the material acquires selectivity of shape and electronic interaction (i.e., with functional groups of polymer) for the desired molecule [39]. MIP systems are in fact also referred as "synthetic receptors."

Another innovation that would be generally useful in radiochemistry but particularly applicable to DOD systems (due to their preferred micronized nature) is the use of supported precursors. These systems should be projected in such a way that the labeling reaction is the only event that would make the molecular structure to become free from the solid support bond. In this way, no other complex organic species will be present in the resulting mixture, and only simple filtration and reformulation steps would be required in order to retrieve the radiopharmaceutical. Some systems based on supported sulfonates [40] or triazene [41] have been reported up to date, and patent literature also refers to examples of supported ionic precursors (e.g., iodonium compounds) [42]. However, none of these systems have demonstrated a preferential use compared to traditional methods, probably because of the mismatch between the support active surface and reagent accessibility to it. The use of micronized systems could be beneficial in solving this mismatch, and indeed the use of sulfonate precursors supported on a monolith structure grown directly in a microfluidic chip gave satisfying yields of radiofluorination [43].

A further modification to this approach, which would facilitate the respect of DOD requirements, could be the use of *reversibly* linked precursors. In this concept, the precursor should form a bond (e.g., covalent coordination) with the support material, and as usual, the labeling reaction should be able to selectively cleave the structure from the support; however, in a second "recycling" step, a change in conditions will allow the recovery of the precursor out of the system and offer a support free to be reversibly functionalized again with a different precursor. A recent paper reported the catalysis by TiO_2 nanoparticles in radiofluorinating a tosylate precursor [44]; interestingly enough, the authors suspect that the process is catalyzed due to selective coordination of the tosylate moiety with the titania surface, therefore opening to the idea of a reversible functionalization of metal nanoparticles with several different precursors prior to radiolabeling. Another possibility, drawn from the field of self-healing materials, might be the use of reversible click reactions, a nice example of which is represented by the 1,2,4-triazoline-3,5-dione chemistry (TAD) moieties. This structure reacts in a reversible way (using different temperatures, Fig. 6.2) with indoles through an ene click reaction [45]; however, it undergoes fast Diels-Alder reactions with dienes and is

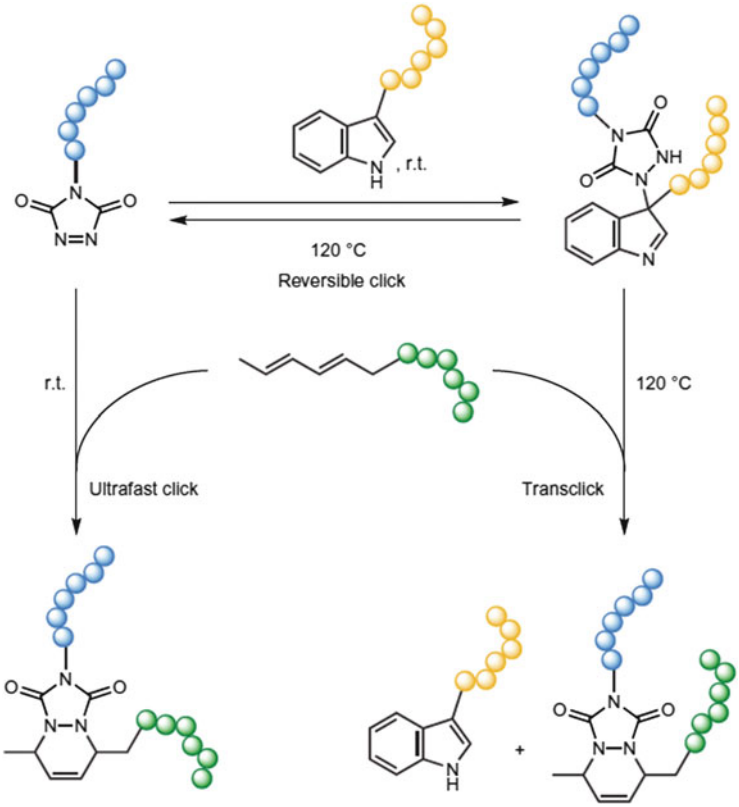

Fig. 6.2 TAD residue in reversible click-chemistry transformations (Taken from [45])

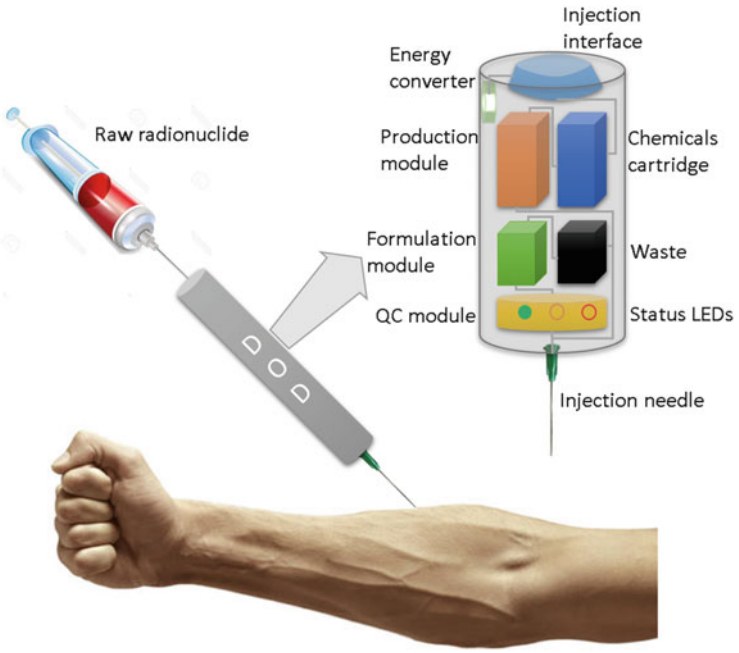

Fig. 6.3 Idealized concept for a DOD system, used to inject directly in the patient the desired radiopharmaceutical

widely used in biology for its capacity to bind irreversibly tyrosine residues [46]. Such an approach could be very useful in DOD processes aimed at protein labeling, for which radiolabeled prosthetic groups enabling click chemistry are now widely employed [47].

Another important point to clarify is whether DOD systems should produce product vials (as in the traditional approach), a syringe/cartridge dose, or even directly deliver the radiopharmaceutical preparation into the vein of the subject (see Fig. 6.3). Though currently unlikely, the possibility to overcome the concept of product vial is very appealing on the base of flexibility, atom efficiency, and procedure streamlining. Therefore, an outstanding challenge is represented by modifying the regulators' view [48, 49] on the requirements needed to prepare injectable radiopharmaceuticals for human use, in order to allow easier and more personalized modalities of dose delivery. One of the ways to achieve such result is represented by the change in quality control (QC) paradigms; in fact, the traditional way to produce a separate vial for QC [50] should be overtaken by the possibility of realizing a DOD process whose precise control and monitoring would represent itself a guarantee of good-quality end product.

6.6 Conclusions

Miniaturization and optimization of the biochemical hardware involved have created a substantial personalization of several medical practices. A typical example of this trend that has improved the treatment of diabetic subjects is the current possibility for any person to check their glucose levels using a straightforward handheld system, instead of reaching the nearest hospital and performing a proper blood examination. This level of simplicity, flexibility, and personalization is currently lacking in the important field of radiopharmaceutical production. However, several studies are starting to demonstrate that new chemical technologies (e.g., microfluidics, high-tech polymers) can represent useful tools to achieve what we can define Dose-On-Demand systems. Several challenges are still to be faced before reaching such a useful target in an efficient and affordable way; we however think that the realization of this capability will be the main way to allow the use of rare and disease dedicated tracers whose widespread utilization is currently hindered [51] by the existing radiopharmaceutical production paradigms.

References

1. Keng PY, Esterby M, van Dam RM. Emerging technologies for decentralized production of PET tracers. In: Positron emission tomography – current clinical and research aspects. 2012. doi:10.5772/1280
2. Satyamurthy N. Electronic generators for the production of positron-emitter labeled radiopharmaceuticals where would PET be without them? Clin Positron Imaging. 1999;2:233–53.
3. Wang M-W, Lin W-Y, Liu K, Masterman-Smith M, Kwang-Fu Shen C. Microfluidics for positron emission tomography probe development. Mol Imaging. 2010;9:175–91.
4. Arima V, Pascali G, Lade O, et al. Radiochemistry on chip: towards dose-on-demand synthesis of PET radiopharmaceuticals. Lab Chip. 2013;13:2328–36.
5. Pascali G, Nannavecchia G, Pitzianti S, Salvadori PA. Dose-on-demand of diverse 18F-fluorocholine derivatives through a two-step microfluidic approach. Nucl Med Biol. 2011;38:637–44.
6. Knapp FF (Russ., Mirzadeh S. The continuing important role of radionuclide generator systems for nuclear medicine. Eur J Nucl Med. 1994;21:1151–65.
7. Welch MJ, Kilbourn MR. A remote system for the routine production of oxygen-15 radiopharmaceuticals. J Label Compd Radiopharm. 1985;22:1193–200.
8. Miller PW, Long NJ, Vilar R, Gee AD. Synthesis of 11C, 18F, 15O, and 13N radiolabels for positron emission tomography. Angew Chem Int Ed Engl. 2008;47:8998–9033.

9. Awasthi V, Watson J, Gali H, Matlock G, McFarland A, Bailey J, Anzellotti A. A "dose on demand" biomarker generator for automated production of [(18)F]F(-) and [(18)F]FDG. Appl Radiat Isot. 2014;89:167–75.
10. Awasthi V, Gali H, McFarland A, Anzellotti A. Automated manufacture of Na[18F]F at the University of Oklahoma Health Sciences Center (OUHSC). Dose on-demand and imaging studies. J Nucl Med. 2014;55:1243.
11. Anzellotti A, Bailey J, Ferguson D, McFarland A, Bochev P, Andreev G, Awasthi V, Brown-Proctor C. Automated production and quality testing of [18F]labeled radiotracers using the BG75 system. J Radioanal Nucl Chem. 2015;305:387–401.
12. Anzellotti A, Yuan H. Automated manufacture of [18F]FMISO in the BG 75 system. Synthesis and purification using solid phase extraction. J Nucl Med. 2015;56:1001.
13. Gali H, Nkepang G, Galbraith W, Hammond K, Awasthi V, Collier TL. Preparation of [F-18] FLT using an ABT compact cyclotron and continuous flow microfluidics. J Label Compd Radiopharm. 2015;58 Suppl 1:S362.
14. Lu S, Giamis AM, Pike VW. Synthesis of [F]fallypride in a micro-reactor: rapid optimization and multiple-production in small doses for micro-PET studies. Curr Radiopharm. 2009;2:49–55.
15. Pascali G, Mazzone G, Saccomanni G, Manera C, Salvadori PA. Microfluidic approach for fast labeling optimization and dose-on-demand implementation. Nucl Med Biol. 2010;37:547–55.
16. Liang SH, Yokell DL, Jackson RN, Rice PA, Callahan R, Johnson KA, Alagille D, Tamagnan G, Collier TL, Vasdev N. Microfluidic continuous-flow radiosynthesis of [(18)F] FPEB suitable for human PET imaging. Medchemcomm. 2014;5:432–5.
17. Collier T, Yokell D, Rice P, Jackson R, Shoup T, Normandin M, Brady T, El Fakhri G, Liang S, Vasdev N. First human use of the tau radiopharmaceutical [18F]T807 by microfluidic flow chemistry. J Nucl Med. 2014;55:1246.
18. Pascali G, Berton A, DeSimone M, Wyatt N, Matesic L, Greguric I, Salvadori PA. Hardware and software modifications on the Advion NanoTek microfluidic platform to extend flexibility for radiochemical synthesis. Appl Radiat Isot. 2014;84:40–7.
19. Matesic L, Kallinen A, Wyatt NA, Pham TQ, Greguric I, Pascali G. [18F]Fluorination optimisation and the fully automated production of [18F]MEL050 using a microfluidic system. Aust J Chem. 2015;68:69–71.
20. Matesic L, Kallinen A, Greguric I, Pascali G. Dose-on-demand production of multiple 18F-radiotracers on a microfluidic system. J Label Compd Radiopharm. 2015;58 Suppl 1:S22.
21. Zheng M-Q, Collier L, Bois F, Kelada OJ, Hammond K, Ropchan J, Akula MR, Carlson DJ, Kabalka GW, Huang Y. Synthesis of [(18)F]FMISO in a flow-through microfluidic reactor: development and clinical application. Nucl Med Biol. 2015;42:578–84.
22. Selivanova SV, Mu L, Ungersboeck J, Stellfeld T, Ametamey SM, Schibli R, Wadsak W. - Single-step radiofluorination of peptides using continuous flow microreactor. Org Biomol Chem. 2012;10:3871.
23. Richter S, Bouvet V, Wuest M, Bergmann R, Steinbach J, Pietzsch J, Neundorf I, Wuest F. (18)F-Labeled phosphopeptide-cell-penetrating peptide dimers with enhanced cell uptake properties in human cancer cells. Nucl Med Biol. 2012;39:1202–12.
24. Bouvet VR, Wuest F. Application of [18F]FDG in radiolabeling reactions using microfluidic technology. Lab Chip. 2013;13:4290–4.
25. Cumming RC, Olberg DE, Sutcliffe JL. Rapid 18 F-radiolabeling of peptides from [18 F] fluoride using a single microfluidics device. RSC Adv. 2014;4:49529–34.
26. Mathiessen B, Zhuravlev F. Automated solid-phase radiofluorination using polymer-supported phosphazenes. Molecules. 2013;18:10531–47.
27. Ismail R, Irribaren J, Javed MR, Machness A, Michael van Dam R, Keng PY. Cationic imidazolium polymer monoliths for efficient solvent exchange, activation and fluorination on a continuous flow system. RSC Adv. 2014;4:25348.
28. Liu K, Lepin EJ, Wang M-W, et al. Microfluidic-based 18F-labeling of biomolecules for immuno-positron emission tomography. Mol Imaging. 2011;10:168–76.
29. Keng PY, Chen S, Ding H, et al. Micro-chemical synthesis of molecular probes on an electronic microfluidic device. Proc Natl Acad Sci U S A. 2012;109:690–5.

30. Javed MR, Chen S, Kim H-K, Wei L, Czernin J, Kim C-JCJ, van Dam RM, Keng PY. Efficient radiosynthesis of 3′-deoxy-3′-18F-fluorothymidine using electrowetting-on-dielectric digital microfluidic chip. J Nucl Med. 2014;55:321–8.
31. Javed MR, Chen S, Lei J, Collins J, Sergeev M, Kim H-K, Kim C-J, van Dam RM, Keng PY. High yield and high specific activity synthesis of [18F]fallypride in a batch microfluidic reactor for micro-PET imaging. Chem Commun (Camb). 2014;50:1192–4.
32. Chen S, Javed MR, Kim H-K, Lei J, Lazari M, Shah GJ, van Dam RM, Keng P-Y, Kim C-JCJ. Radiolabelling diverse positron emission tomography (PET) tracers using a single digital microfluidic reactor chip. Lab Chip. 2014;14:902–10.
33. Ali I, Aboul-Enein HY, Gupta VK. Nanochromatography and nanocapillary electrophoresis. 2009. doi:10.1002/9780470434925
34. Ghanem A, Ikegami T. Recent advances in silica-based monoliths: preparations, characterizations and applications. J Sep Sci. 2011;34:1945–57.
35. Wouters B, De Vos J, Desmet G, Terryn H, Schoenmakers PJ, Eeltink S. Design of a microfluidic device for comprehensive spatial two-dimensional liquid chromatography. J Sep Sci. 2015;38:1123–9.
36. Zhou D, Chu W, Peng X, McConathy J, Mach RH, Katzenellenbogen JA. Facile purification and click labeling with 2-[18F]fluoroethyl azide using solid phase extraction cartridges. Tetrahedron Lett. 2015;56:952–4.
37. Fedorova O, Kuznetsova O, Stepanova M, Maleev V, Belokon Y, Wester H-J, Krasikova R. A facile direct nucleophilic synthesis of O-(2-[18F]fluoroethyl)-l-tyrosine ([18F]FET) without HPLC purification. J Radioanal Nucl Chem. 2014;301:505–12.
38. Turiel E, Martín-Esteban A. Molecularly imprinted polymers for sample preparation: a review. Anal Chim Acta. 2010;668:87–99.
39. Haupt K, Mosbach K. Molecularly imprinted polymers and their use in biomimetic sensors. Chem Rev. 2000;100:2495–504.
40. Brown LJ, Bouvet DR, Champion S, et al. A solid-phase route to18F-labeled tracers, exemplified by the synthesis of [18F]2-Fluoro-2-deoxy-D-glucose. Angew Chemie. 2007;119:959–62.
41. Riss PJ, Kuschel S, Aigbirhio FI. No carrier-added nucleophilic aromatic radiofluorination using solid phase supported arenediazonium sulfonates and 1-(aryldiazenyl)piperazines. Tetrahedron Lett. 2012;53:1717–9.
42. Brady F, Luthra S, Robins E. Solid-phase fluorination of uracil and cytosine. 2006. US 10/538,904.
43. Ismail R, Machness A, van Dam RM, Keng P-Y. Solid-phase [18F]fluorination on a flow-through glass microfluidic chip. In: 16th int. conf. miniaturized syst. chem. life sci. 2012. Okinawa, Japan, p. 629–631
44. Sergeev ME, Morgia F, Lazari M, Wang C, van Dam RM. Titania-catalyzed radiofluorination of tosylated precursors in highly aqueous medium. J Am Chem Soc. 2015;137:5686–94.
45. Billiet S, De Bruycker K, Driessen F, Goossens H, Van Speybroeck V, Winne JM, Du Prez FE. Triazolinediones enable ultrafast and reversible click chemistry for the design of dynamic polymer systems. Nat Chem. 2014;6:815–21.
46. Ban H, Nagano M, Gavrilyuk J, Hakamata W, Inokuma T, Barbas CF. Facile and stabile linkages through tyrosine: bioconjugation strategies with the tyrosine-click reaction. Bioconjug Chem. 2013;24:520–32.
47. Kim DW. Bioorthogonal click chemistry for fluorine-18 labeling protocols under physiologically friendly reaction condition. J Fluor Chem. 2015;174:142–7.
48. Salvadori AP. Radiopharmaceuticals, drug development and pharmaceutical regulations in Europe. Curr Radiopharm. 2015;1:7–11.
49. VanBrocklin FH. Radiopharmaceuticals for drug development: United States regulatory perspective. Curr Radiopharm. 2015;1:2–6.
50. Yu S. Review of 18F-FDG synthesis and quality control. Biomed Imaging Interv J. 2006;2:e57.
51. Reilly RM, Lam K, Chan C, Levine M. Advancing novel molecular imaging agents from preclinical studies to first-in-humans phase I clinical trials in academia – a roadmap for overcoming perceived barriers. Bioconjug Chem. 2015;26:625–32.

Chapter 7
Advantages of Radiochemistry in Microliter Volumes

Pei Yuin Keng, Maxim Sergeev, and R. Michael van Dam

Abstract Positron emission tomography (PET) provides quantitative 3D visualization of physiological parameters (e.g., metabolic rate, receptor density, gene expression, blood flow) in real time in the living body. By enabling measurement of differences in such characteristics between normal and diseased tissues, PET serves as vital tool for basic research as well as for clinical diagnosis and patient management. Prior to a PET scan, the patient is injected with a short-lived tracer labeled with a positron-emitting isotope. Safe preparation of the tracer is an expensive process, requiring specially trained personnel and high-cost equipment operated within hot cells. The current centralized manufacturing strategy, in which large batches are prepared and divided among many patients, enables the most commonly used tracer (i.e., [^{18}F]FDG) to be obtained at an affordable price. However, as the diversity of tracers increases, other strategies for cost reduction will become necessary. This challenge is being addressed by the development of miniaturized radiochemistry instrumentation based on microfluidics. These compact systems have the potential to significantly reduce equipment cost and shielding while increasing diversity of tracers produced in a given facility. The most common approach uses "flow-through" microreactors, which leverage the ability to precisely control reaction conditions to improve synthesis times and yields. Several groups have also developed "batch" microreactors which offer significant additional advantages such as reduced reagent consumption, simpler purifications, and exceptionally high specific activity, by reducing operating volumes by orders of magnitude. In this chapter, we review these "batch" approaches and the advantages of using small volumes, with special emphasis on digital microfluidics, in which reactions have been performed with volumes as low as ~1 μL.

Keywords Microfluidics • Radiosynthesis • Positron emission tomography (PET) • Electrowetting-on-dielectric (EWOD) • Microscale chemistry

P.Y. Keng • M. Sergeev • R.M. van Dam (✉)
Crump Institute for Molecular Imaging and Department of Molecular and Medical Pharmacology, David Geffen School of Medicine, University of California, Los Angeles, CA, USA
e-mail: mvandam@mednet.ucla.edu

Y. Kuge et al. (eds.), *Perspectives on Nuclear Medicine for Molecular Diagnosis and Integrated Therapy*, DOI 10.1007/978-4-431-55894-1_7

7.1 Introduction

7.1.1 Radiosynthesis of Positron Emission Tomography Tracers

Positron emission tomography (PET) is an extremely powerful, noninvasive diagnostic imaging technology capable of measuring a plethora of biological processes in vivo [1]. In research, PET can provide dynamic information about normal or diseased states of a living organism and, in the clinic, can provide information that is critical for diagnosis, selection of therapy, or monitoring response to therapy. In some cases, PET can detect biochemical changes associated with disease before any anatomical changes can be observed [2].

PET requires injection of a tracer labeled with a positron-emitting isotope, such as fluorine-18, nitrogen-13, oxygen-15, carbon-11, or a radiometal. Fluorine-18 possesses physical and nuclear properties that are particularly desirable for radiolabeling and imaging [3]. For example, the low positron energy and range ensure high-resolution imaging while minimizing radiation exposure to the patient. In addition, the 110 min half-life is sufficiently long for multistep synthesis, transport to the imaging site, and imaging over extended periods.

Due to the hazard of working with radioactive materials, a specialized infrastructure of automated radiosynthesizers operating in radiation-shielded "hot cells" by expert personnel is required. Due to the high costs, a couple of tracers (including 2-[^{18}F]fluoro-2-deoxy-D-glucose, [^{18}F]FDG) are currently produced in a "satellite" manner. Radiopharmacies manufacture large batches that are subdivided among many patients within a local area to leverage economies of scale and offer the compound at an affordable price. As the diversity of PET tracers used in medical care and research increases, opportunities to share costs are reduced, and alternative innovative approaches are needed to reduce the high cost of each batch.

A particularly promising approach is the development of miniaturized radiosynthesizers based on microfluidic technology that can enable dramatic reductions in the cost of equipment and the amount of radiation shielding needed. An additional innovation is the concept of disposable "cassettes," which allows each synthesizer to make a wide range of tracers simply by using different cassettes, rather than being dedicated to production of a single tracer [4].

7.1.2 Microfluidics for Radiosynthesis

It has been well established that the geometry of microfluidic devices offers many advantages for the synthesis of short-lived radiopharmaceuticals [5–7]. In particular, the small dimensions enable improved control of reaction conditions via rapid mixing and efficient heat transfer, leading to faster reactions and improved selectivity, thus higher yields.

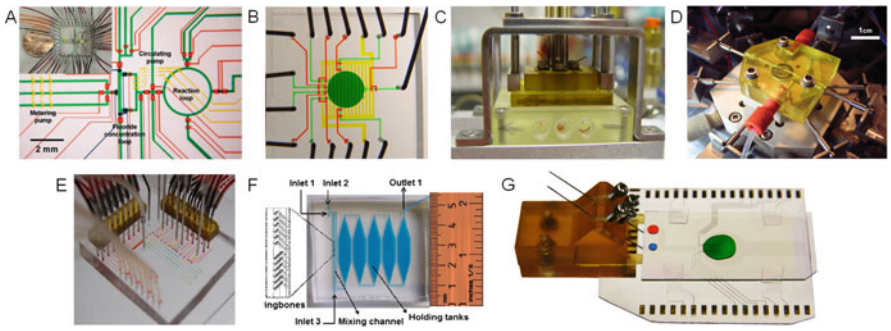

Fig. 7.1 Batch microfluidics devices for synthesis of PET tracers: (**a**) PDMS chip with 40 nL reactor (Adapted from reference [14] with permission from AAAS). (**b**) Scaled-up PDMS chip with 5 μL reactor (Adapted from reference [15], Copyright © 2010 by the Society of Nuclear Medicine and Molecular Imaging, Inc.). (**c**) Chemically inert polydicyclopentadiene (pDCPD) polymer chip with 5 μL reactor (Reproduced from reference [56]). (**d**) Chemically inert pDCPD chip with 60 μL reactor (Reproduced with permission from reference [50], Copyright © 2010 John Wiley & Sons, Ltd.). (**e**) PDMS chip for optimizing radiolabeling reaction in variable volume droplets (~100 nL) (Reproduced with permission from reference [59], Copyright © 2015 IOP Publishing). (**f**) PDMS chip for radiometal labeling with 25 μL reaction volume (Reproduced with permission from reference [19], Copyright © 2013 Elsevier, Inc.) (**g**) EWOD chip with reaction volume ranging from 2 to 17 μL

Most commonly in the field of radiochemistry, these devices are based on "flow-through" microreactors, where reactions occur by flowing reagent streams through mixers and preheated capillary tubes or microchannels. Numerous groups have demonstrated the radiosynthesis of [^{18}F]FDG in polymer chips [8], glass chips [9], and capillary tubes [10]. This technology has been commercialized (e.g., Advion Biosciences "NanoTek" and Scintomics "μ-ICR"), and dozens of different radiotracers labeled with F-18, C-11, N-13, and Tc-99 m have been demonstrated [11]. Recent advances have enabled the integration of solvent exchange processes [12, 13], which previously were accomplished via bulky, off-chip subsystems.

Because it is important that flow-through systems are completely filled with liquid in order to achieve accurate fluid handling, typical operating volumes are comparable to macroscale systems (i.e., >500 μL). Another class of microfluidic device based on small (<50 μL) volumes known as "batch" microreactors have also been used for radiochemistry (Fig. 7.1). These devices are particularly attractive for radiochemistry because all synthetic steps including solvent exchange can be integrated into a single chip and because small volumes can reduce reagent consumption, enhance reaction kinetics, improve specific activity, reduce radiolysis, and simplify purification, as described below.

7.1.3 Platforms for Microliter Volume Synthesis

The first batch microfluidic synthesis of [^{18}F]FDG was demonstrated in a polydimethylsiloxane (PDMS) chip with 40 nL reaction volume [14]. Microvalves

were used to close the reactor during reaction steps, and the permeability of the PDMS enabled escape of vapor for solvent exchange processes. By scaling up the reactor volume to 5 μL, it was possible to produce mCi amounts of [^{18}F]-labeled tracers [15]. Unfortunately, due to adverse interaction of PDMS with [^{18}F]fluoride [16], radioactivity losses were high and reliability was low. Using inert plastic materials as the reaction vessel improved reliability, and a system with 50 μL reaction volume enabled production of tracers of sufficient quantity and quality for human imaging [17], establishing the relevance of the micro-batch format.

While the PDMS chip was not suitable for processing [^{18}F]fluoride, the capability to react small volumes was found to be useful for screening radiolabeling conditions for the reaction of [^{18}F]SFB with an engineered antibody [18]. Using $<$100 nL per droplet, many reaction conditions could be tested, and then the whole batch could be labeled once optimal conditions were found. A quasi-continuous-flow PDMS chip using small volumes (25 μL) has also been used for radiolabeling peptides and proteins with radiometals such as Ga-68 and Cu-64 [19]. The small volume enabled improved stoichiometry of the label and ligand, dramatically improving the labeling yield and potentially avoiding the need for extensive purification.

Recently, our group demonstrated successful radiosynthesis of [^{18}F]FDG and other molecules using another type of batch microfluidic device based on the digital manipulation of droplets between two parallel plates [20, 21] known as electrowetting-on-dielectric (EWOD). Droplets are controlled by on-chip electrodes (Fig. 7.2), eliminating the need for bulky valve actuators, pumps, and radiation shielding as is needed in the approaches mentioned above. A wide range of reagents and reaction conditions can be used on these EWOD microchips because they are constructed from inert and thermally stable materials (glass substrate, metallic electrode layer, inorganic dielectric layer, and fluoropolymer layer). Because droplets are surrounded by gas, evaporation and solvent exchange can readily be performed on the chip. Resistive heating, temperature sensing for precise temperature control, and impedance sensing for measuring electrical properties of liquid can all be integrated on the chip without the need of additional bulky hardware [22].

Using this platform, our laboratory has reported the successful synthesis of [^{18}F]FDG [20], 3-[^{18}F]fluoro-3′-deoxy-fluorothymidine ([^{18}F]FLT) [23], [^{18}F]fallypride [24], and N-succinimidyl 4-[^{18}F]fluorobenzoate ([^{18}F]SFB) [25] with radiochemical yields of 22 ± 8 % ($n = 11$), 63 ± 5 % ($n = 5$), 65 ± 6 % ($n = 7$), and 19 ± 8 % ($n = 5$), respectively. The final ^{18}F-labeled compounds passed all quality control tests required by the United States Pharmacopeia for injection into humans and have been successfully used in preclinical PET. The syntheses of [^{18}F]FDG and [^{18}F]FLT on a simplified EWOD chip have also been reported by others [26, 27]. These results suggest that the EWOD-based synthesizer can meet the requirements for on-demand production of diverse PET tracers to meet preclinical or clinical needs.

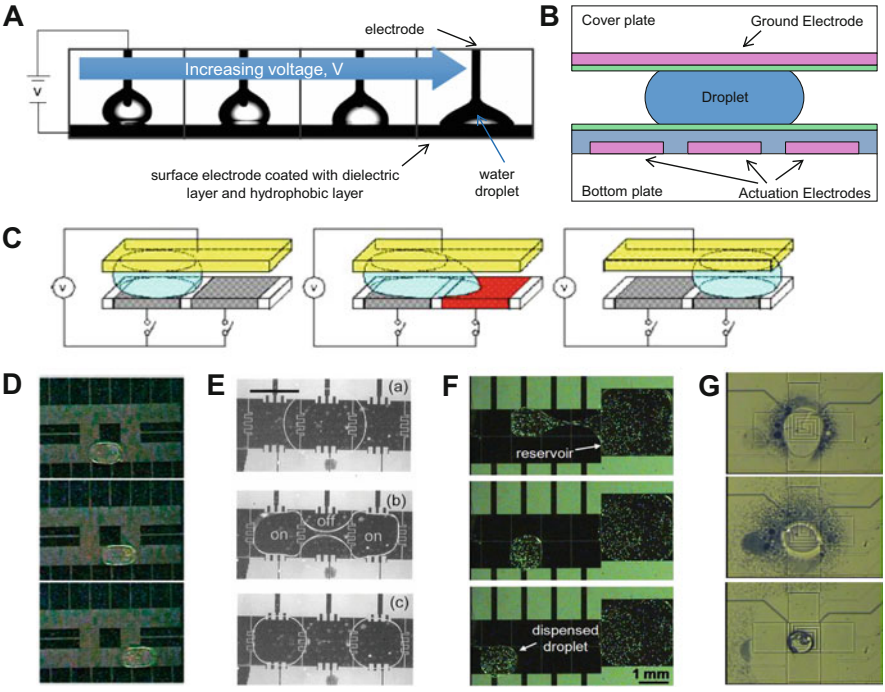

Fig. 7.2 Structure and operation of EWOD microfluidic chips. (**a**) Illustration of the "electrowetting" effect. (**b**) Schematic of typical EWOD device with droplet sandwiched between the two plates. (**c**) Applying a local field to one end of the droplet using a small control electrode (typically 1 or 2 mm square) can generate a force on the droplet in a direction toward the activated electrode (Diagram courtesy of Robin Garrell). This force enables several operations, including (**d**) droplet transport along a predetermined path, (**e**) droplet splitting, and (**f**) droplet dispensing from an on-chip reservoir. Incorporation of specialized heating electrodes permits additional operations such as (**g**) evaporation of solvent. ((d) is reproduced with permission from reference [60] (Copyright © 2004 American Chemical Society), (e) is reproduced with permission from reference [61] (Copyright © 2003 IEEE), (f) is reproduced from reference [62] with permission of The Royal Society of Chemistry.)

7.2 Advantages of Radiosynthesis at the Microliter Scale

7.2.1 Miniaturization and Disposability

Perhaps the most significant potential advantage of batch microfluidics in the field of radiochemistry is the potential to integrate the entire synthesis, purification, and formulation apparatus into an extremely compact system. Size of the components that need to be shielded (because they contain or contact radioactivity) has a tremendous impact on the amount of radiation shielding needed. For a constant thickness "shell" of shielding, t, the volume (and weight and cost) of the shielding scale is

$$\begin{aligned}\text{Shielding volume} \sim (r+t)^3 - r^3 &= (3r^2t + 3rt^2 + t^3) \\ &= 3r^2t\left(1 + \frac{t}{r} + \frac{1}{3}\frac{t^2}{r^2}\right)\end{aligned}$$

where r is the dimension of the synthesizer. Assuming a fixed shielding thickness where $t \ll r$, the scale factor is proportional to r^2. Thus, moving from macroscale systems with ~20-inch dimensions to microfluidic chips with ~2-inch dimensions can reduce the needed shielding 100-fold. This reduction could make it practical for radiochemistry chips to be used in benchtop situations instead of needing to operate them in specialized facilities equipped with hot cells and mini cells to shield radiation, thus removing one of the bottlenecks in PET tracer production.

Integrating the fluid pathways of a radiosynthesizer into a microfluidic chip has other advantages as well. If the chip can be made to be very inexpensive, the entire fluid pathway can be discarded after each synthesis run, eliminating the need for developing and validating a cleaning protocol and associated documentation or cleaning the system on a daily basis. This concept of disposability is increasingly being used in macroscale synthesizers to simplify setup, cleanup, and compliance with cGMP manufacturing guidelines for PET tracers that are used in humans [4]. Disposable cassettes also provide flexibility: with a single synthesizer instrument, the operator can choose to install different disposable cassettes (with different pre-configured fluid path configurations) along with matching reagent kits to make different PET tracers [4].

7.2.2 *Reduced Radiolysis*

Radiolysis is the process of chemical bond cleavage caused by radiation. Molecules of a PET probe undergo irradiation from both the starting [^{18}F]fluoride (external radiolysis) and from other radiolabeled molecules (autoradiolysis) [28–30], which can lead to reduction in the yield of the probe and the formation of radioactive side products. The mechanism of damage is believed to be related to the formation of radical species in the solvent by high-energy particles [29]. While the final injectable formulation can be stabilized against autoradiolysis with addition of radical scavengers (*e.g.*, ethanol) to preserve radiochemical purity [30], this is not generally possible at earlier stages during the radiosynthesis process.

Fluorine-18 emits positrons with high energy ($E_{max} = 0.633$ MeV) that cause ionization of the solvent while dissipating their kinetic energy along their travel range. The range is up to ~2.4 mm, but due to the tortuous path they follow, the distribution of final displacements of positrons from their origin is characterized by a smaller range (i.e., full width at one third maximum ~1 mm) [31]. When the reaction vessel dimensions (e.g., vial, flask, or Eppendorf tube: ~10 mm) are much greater than this range, each positron deposits all of its energy into the solvent, leading to extensive radiolysis (Fig. 7.3a).

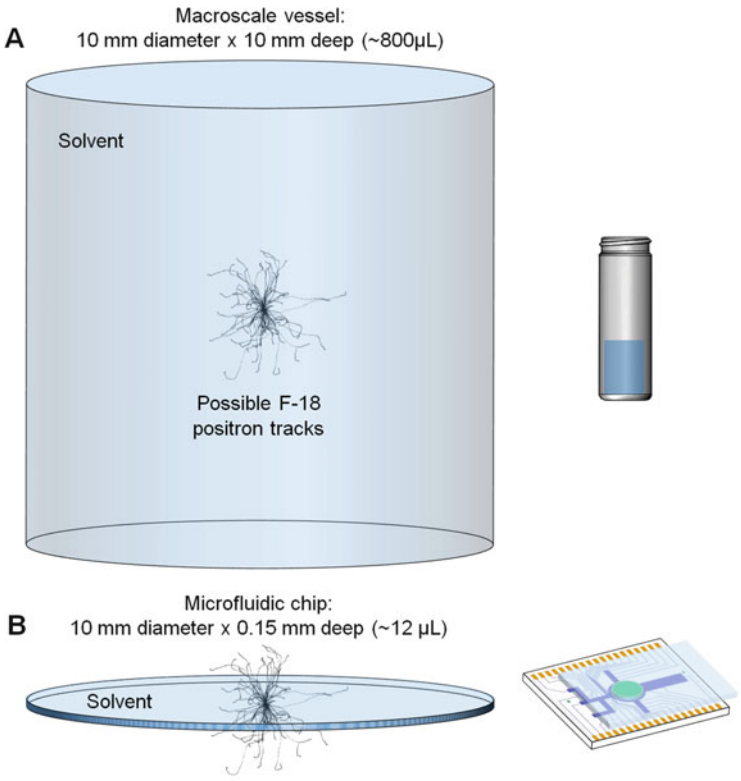

Fig. 7.3 Illustration of radiolysis suppression. (**a**) Possible positron tracks from decay of a fluorine-18 atom at the center of a conventional macroscale reaction vessel. Because the positron range is significantly less than the reactor dimensions, the positron will deposit all of its energy into the solvent, where it causes radiolysis. This is true of decay events happening throughout the vial. (**b**) In contrast, in an EWOD microfluidic chip, one dimension of the solvent volume is very thin compared to the positron range. Thus, a significant portion of the possible tracks are mostly or entirely outside the droplet. Thus, most positrons will escape the solvent after having only deposited a small fraction of their energy in the solvent, reducing radiolysis

Rensch et al. have shown via simulations and experiments that the degree of radiolysis is geometry dependent [3]. In vessels for which at least one dimension is significantly smaller than the positron range (e.g., capillary tubing or EWOD chips), there is significantly reduced radiolysis because positrons can escape the solvent before depositing very much of their energy (Fig. 7.3b). For example, the solvent within a 100 µm diameter capillary reactor absorbs only 10 % of the energy

of positrons emitted from within the solvent, and a planar droplet geometry with 100 μm height (similar to the EWOD chip) absorbs only 40 % of the positron energy [32]. Further reduction could be achieved by reducing the dimensions.

7.2.3 Reagent Minimization

Because batch microfluidic chips such as EWOD handle volumes that are 2–3 orders of magnitude less than conventional systems, the quantity of reagents needed to perform reactions is proportionately reduced, thereby reducing the per-run reagent cost. Generally the precursor is the most expensive reagent. In macroscale synthesis, reagents for common small-molecule PET tracers can cost hundreds of US$ for a single synthesis run (e.g., 10 mg in ~1 mL). Synthesis in microliter volumes (e.g., 10–100 μg precursor) could reduce this cost down to dollars per run (depending on costs of packing this small amount of reagent into vials), making it economical to produce even small batches on demand for a single user. Biomolecule-based precursors such as proteins are even more expensive, costing up to thousands of US$ for a single synthesis. Using microliter volumes, the 100 s of micrograms quantity typically used for protein labeling could be reduced to microgram or submicrogram levels. Reducing the reagent consumption enables a greater number of runs per a given amount of precursor or reduces the cost per run of precursor.

Minimization of reagents can also simplify purification processes [19]. Typically in ^{18}F-radiochemistry, the amount of precursor is many of orders of magnitude higher than the amount of [^{18}F]fluoride to ensure the fluorination reaction occurs as rapidly as possible. For example, in the synthesis of [^{18}F]FDG, one typically uses about 40 μmol of mannose triflate [33], compared to the 600 pmol of [^{18}F]fluoride ion in a 1000 mCi batch, representing an excess of 5 orders of magnitude. Even accounting for typical final specific activity, the amount of [^{19}F]fluoride + [^{18}F]fluoride is about 60–600 nmol, meaning there is still an excess of about 2–3 orders of magnitude of precursor compared to ([^{18}F] + [^{19}F])FDG. This means that at the end of the synthesis, there are vast amounts of unreacted (or hydrolyzed) precursor that must be separated from a much smaller amount of the desired product. Because of the high amounts or precursor, large reaction volume, and the chemical similarity between precursor (native or hydrolyzed) and product, long semi-preparative HPLC purification times may be needed, resulting in a large solvent volume in the purified product. While suitable for patient use, these large volumes can be problematic for imaging in small animals, where the tracer must be sufficiently concentrated to inject enough radioactivity for imaging (typically 100–200 μCi) within the maximum recommended injection volume to avoid physiological perturbation (e.g., <100 μL for mice). Using smaller amounts of reagents in microfluidic formats, several groups have demonstrated that analytical-scale HPLC is sufficient for purification [24, 34], resulting in more concentrated final

formulation. Purification has also been successfully performed with on-chip structures similar to typical macroscale Sep-Pak cartridges [35–37].

Reduced amount of reagents may also simplify the quality control (QC) testing that is needed prior to injection in humans. In general, the reduced amounts of reagents and solvents will lead to reduced amounts of residual impurities after the purification process. An interesting prospect of using extremely tiny volumes is that if the total amount of reagent added is below the injectable limits set by various regulatory agencies, then a test for the absence of that particular chemical may become unnecessary.

7.2.4 High Specific Activity

The specific activity (SA) of a PET tracer (e.g., labeled with fluorine-18) is defined as the ratio of the number of ^{18}F-labeled molecules to the total number of ^{18}F-labeled and ^{19}F-labeled molecules and is typically reported in units of radioactivity per mass (e.g., Ci/μmol). For a certain desired injected dose (e.g., 10 mCi for humans), the higher the SA, the lower the mass that is injected.

High SA of a PET tracer is important for several reasons. First, because many PET tracers are based on pharmacologically active compounds, only a very low mass should be injected to avoid eliciting a pharmacological response. Second, for tracers that target low-abundance receptors (e.g., in neurological imaging), injecting lower mass avoids saturation or high occupancy of the receptors. This is especially important in small animal imaging, in which significantly higher radioactivity is injected (per mass of the animal) compared to human subjects to achieve sufficient image quality with the higher resolution (smaller voxel size) scanners that are used for animals [38]. Third, high SA may improve image quality by increasing the proportion of targets occupied by radioactive forms of the tracer while reducing competitive interactions of the nonradioactive forms. Other reasons to maximize SA are related to the logistics of PET tracer production. Often, tracers need to be transported from the radiopharmacy where they are produced to the imaging center. Because of the radioactive decay during this transport time, the SA is reduced by a factor of 2 for each half-life, and a high initial SA is needed to ensure sufficient SA at the time of imaging.

For fluorine-18, the maximum theoretical SA is 1710 Ci/μmol; however, the actual SA of the final tracer is significantly lower, typically 1–10 Ci/μmol [39]. This means the number of fluorine-18 atoms is dwarfed (~200–2000X) by the number of fluorine-19 contaminant atoms. Some of the fluorine-19 contamination originates due to the equipment and materials used in the [^{18}F]fluoride production process (e.g., [^{18}O]H_2O quality, volume of target, target materials, tubing materials, target loading/unloading process, etc.) [40–42]. While such sources may be out of most radiochemists' control, another significant contribution is the contamination of reaction mixture with extra fluorine-19 fluoride during the synthesis process itself (i.e., all steps upstream of and including the fluorination step). The main sources are the QMA cartridges used in the fluoride drying process, fluorinated materials (e.g.,

Teflon tubing and stirbars) [43], and the reagents used in the synthesis, such as K_2CO_3, Kryptofix, etc.

In preliminary studies, our group observed that microfluidic synthesis on EWOD chips resulted in significantly higher (up to 25–50 times) SA compared to macroscale synthesis, starting with the same amount of radioactivity [23, 24]. This suggested the potential for microfluidics to significantly reduce fluorine-19 contamination in the synthesis process. An in-depth investigation led to the observation that the dependence of SA on reaction parameters was very different for macroscale (100–5000 μL) and microscale (2–8 μL) syntheses. At the macroscale, the SA strongly varied with the reaction volume (amount of reagents) as well as the starting radioactivity (from 10s to 100 s of mCi), whereas the SA was much higher and nearly constant (20–23 Ci/μmol), under all conditions when performed in microdroplets. These results suggest that in the macroscale synthesis, reagents and solvents are the dominant source of fluorine-19, while in microscale volumes, these sources have been nearly eliminated and the fluorine-19 contribution from the cyclotron dominates [44, 45] (Fig. 7.4). The effect of the 120 nm Teflon layer on the chip was also investigated and no impact on SA was seen [43], perhaps due to the radiolysis suppression effect described above.

Small volumes are extremely beneficial for another type of reaction, namely, isotopic exchange (IEX). In IEX reactions, the precursor is identical to the final product, except for the presence of fluorine-19 instead of fluorine-18, and cannot be separated after synthesis. Thus it is desirable to minimize the amount of excess precursor to maintain high SA. In macroscale reactions this is difficult, because the

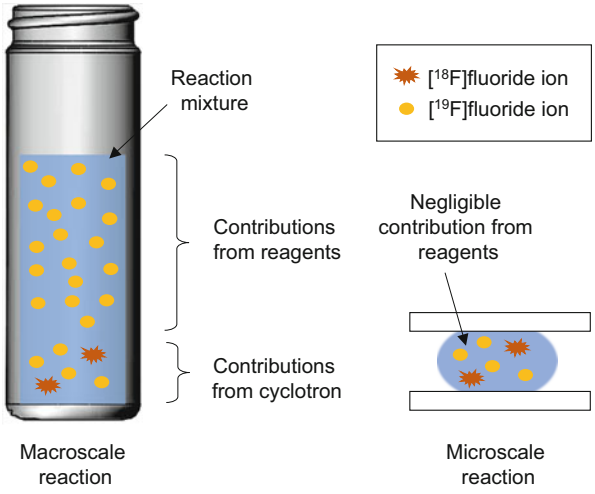

Fig. 7.4 Illustration of specific activity improvement. (*Left*) At the macroscale, reagents are the dominant source of fluorine-19 contamination in the fluorination reaction mixture. (*Right*) At the microscale, the reagents add negligible fluorine-19 contamination to that already present from the cyclotron. After the fluorination reaction, the fluoride (both F-18 and F-19 forms) get incorporated into the precursor and cannot be separated, resulting in ^{18}F- and ^{19}F-labeled forms of the tracer

concentration of precursor needs to be sufficiently high for efficient reaction. However, Perrin et al. have shown that small volume reactions are an effective way to minimize precursor amount for IEX reactions [46, 47]. It should be noted that the same principles can be applied to other carrier-added situations or to the labeling of proteins or other species where the labeled and unlabeled forms cannot be separated; in all such cases, it is critical to minimize the starting material in order to obtain high SA. The dependence of SA on starting radioactivity for IEX reactions was investigated in simplified EWOD chips using rhodamine clicked to an aryl-BF_3 moiety [44]. Unlike in nucleophilic substitution reactions, SA of microfluidic IEX reactions was found to vary with starting radioactivity, but in a nonlinear manner. This suggests that perhaps the contribution of fluorine-19 from the cyclotron is comparable to other sources and further reduced volume may be beneficial.

For both nucleophilic substitution and IEX reactions, small volume synthesis can achieve high SA even from low starting amounts of radioactivity. This is in contrast to macroscale synthesis, where high SA production typically requires starting with Ci levels of radioactivity. Depending on the amount of tracer radioactivity needed, small volume synthesis could therefore reduce the time/cost of cyclotron bombardment, increase safety, and decrease the required amount of shielding required for production.

7.3 Practical Considerations

7.3.1 Limits of Volume Reduction

Clearly there are enormous advantages to performing radiochemistry in small volumes. The current EWOD chip geometry can reliably handle volumes as small as ~2 μL, which is limited by the size of the electrodes that are used to load and transport reagent droplets. Scaling down the volume of radiochemical reactions below 2 μL could enable further reductions in precursor cost, further improvements in specific activity (for IEX reactions or biomolecule labeling), further simplification of purification and QC testing, or reduction in the size of the EWOD chip, which leads to cost reduction. Even smaller droplets could be manipulated by scaling down the electrode size and/or reducing the gap between the chip plates. In fact, using specialized fabrication techniques, Nelson and Kim have shown that droplets as small as 100 pL can be manipulated in an EWOD chip [48].

As the volume is scaled down, it is important to be mindful of several issues. First, a certain minimum volume will be needed to solvate the desired amount of the radioisotope complexed with phase transfer catalyst along with the precursor. Another limitation will be the droplet lifetime: at extremely small volume scales, droplets quickly evaporate and may not last sufficiently long to carry out the fluorination reaction. The limit of volume reduction for radiochemistry applications remains to be explored.

7.3.2 Radioisotope Concentration

When considering using small reaction volumes, one must also consider how to produce sufficient quantity (radioactivity) of the tracer for the particular application needed. For preclinical imaging, generally a few mCi is sufficient for a study involving several animals, and with modern scanners, <25–50 μCi is sufficient for a single mouse. On the other hand, imaging of a single patient requires on the order of 10 mCi, while producing a large batch in a radiopharmacy for distribution to imaging centers would require 100s–1000s of mCi. Even higher amounts of the radioisotope are needed at the beginning of the synthesis due to nonideal yields and fluid handling, as well as losses due to decay.

Cyclotrons can readily generate multiple Ci levels of [^{18}F]fluoride in [^{18}O]H_2O to satisfy any of these applications. However, the output volume is typically in the milliliter range, while the capacity of the current EWOD chip (12 mm diameter reaction zone x 150 μm droplet height) is only ~17 μL, i.e., 1 % of the volume from the cyclotron. From a high-radioactivity bombardment, it would be possible to load as much of tens of mCi of radioisotope into the chip without special measures, but it is not desirable to waste the majority of the radioisotope, and several methods for efficiently concentrating the radioisotope have been developed (Fig. 7.5a).

One approach is to concentrate the [^{18}F]fluoride prior to loading it into the chip via a solid-phase extraction (SPE) process. First, the [^{18}F]fluoride/[^{18}O]H_2O is flowed through a strong anion exchange cartridge (e.g., quaternary methyl ammonium, QMA) to trap the [^{18}F]fluoride. After removing residual water (e.g., with an inert gas flow), an eluent solution (e.g., aqueous K_2CO_3/ $K_{2.2.2}$ or tetrabutylammonium bicarbonate (TBAB), sometimes with MeCN) is passed through the cartridge to release the [^{18}F]fluoride. If the cartridge has sufficiently small bed volume, the volume of eluent solution needed to efficiently collect the [^{18}F]fluoride can be quite low. For example, using commercial cartridges (OPTI-LYNX, Optimize Technologies), Elizarov et al. concentrated 92 % of 876 mCi starting [^{18}F]fluoride into a ~5 μL volume [15], our group demonstrated release into ~12 μL volume [49], and Lebedev et al. [17] and Bejot et al. [50] demonstrated release into 44 μL volume. This approach can be integrated with microfluidics by using packed-tubing cartridges [15], functionalized porous polymer monoliths [51], packed microchannels [52], or resin-filled inserts [12]. Control of trapping and release processes requires the use of valves with small internal volumes to choose which solution is flowed into the cartridge inlet (i.e., [^{18}F]fluoride or eluent) and whether the cartridge outlet is direct to an [^{18}O]H_2O collection reservoir or the microfluidic chip. Most commonly, this is accomplished with HPLC injection valves, but can also be achieved with on-chip microvalves if they can be conveniently integrated into the device (Fig. 7.5b, c). Once loaded into the chip, the concentrated [^{18}F]fluoride solution is generally evaporated to dryness, and then the subsequent fluorination reaction volume can be controlled by the volume of precursor solution added, provided there is sufficient solvent to dissolve not only the precursor but also the fluoride complex with phase transfer catalyst. Similar trap and release of [^{18}F]fluoride can be accomplished with microfluidic electrochemical flow cells

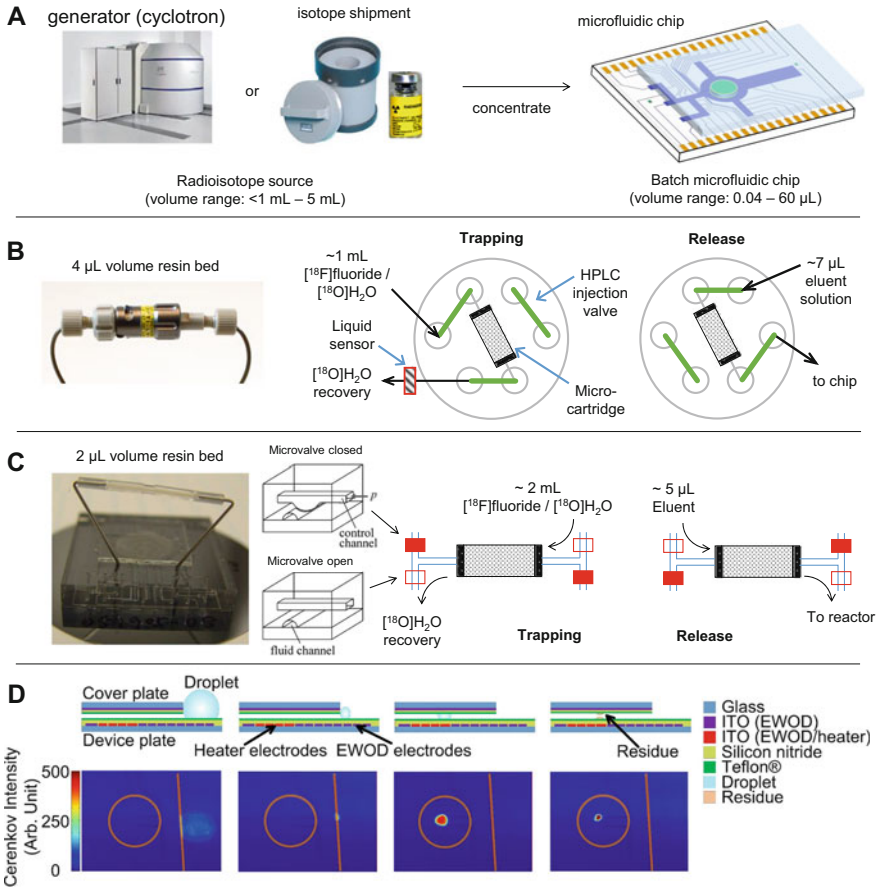

Fig. 7.5 (**a**) Because the volume of batch microfluidic chips is much smaller than the volume of the radioisotope source, concentration is necessary to ensure sufficient quantity of radioactivity can be loaded onto the chip. (**b**) Cartridge-based method for concentration described in Ref. [49]. Using an HPLC injection valve with small internal volume, the flow path can be configured in trapping mode, where the [^{18}F]fluoride/[^{18}O]H_2O is flowed through a micro-cartridge and the [^{18}F] fluoride trapped, or a release mode, where a small volume of eluent solution is passed through the cartridge to release the [^{18}F]fluoride and deliver it onto the chip. (**c**) Cartridge-based method using on-chip microvalves implemented in a polydimethylsiloxane (PDMS) chip. Pressure applied to "control channels" can open or close nearby "fluid channels" to configure the flow path into trapping and release modes (Adapted from reference [15] © by the Society of Nuclear Medicine and Molecular Imaging, Inc.). (**d**) Scheme for evaporative concentration of [^{18}F]fluoride radioisotope. The *top images* show cross-sectional schematics of the concentration process, and the *bottom images* show Cerenkov (radioactivity) images of the *top view* of the chip at corresponding times. *Orange lines* and *circles* were added to depict the cover plate edge and the reaction site, respectively. Initially, a 200 µL droplet of [^{18}F]fluoride solution is loaded to the cover plate edge. By activating a nearby heater, the volume of the droplet is reduced to ~5 µL and then pulled into the chip by electrode actuation. (Reproduced from Ref. [25] with permission from the Royal Society of Chemistry.)

[53, 54] where the [^{18}F]fluoride is trapped at an electrode surface by application of positive voltage.

A different approach is to perform the [^{18}F]fluoride concentration directly on chip [25]. A special chip was fabricated where the bottom plate extended beyond the edge of the cover plate to create a platform. A large droplet of [^{18}F]fluoride solution (with phase transfer catalyst) was loaded onto this platform adjacent to the gap between the two EWOD chip plates and then rapidly evaporated down to a small volume that could be transported between the plates (Fig. 7.5d). Because some groups have reported that the anion exchange resin can contribute fluorine-19 contamination [55], this approach may reduce the amount of fluorine-19 in the reaction mixture and thus enable production of PET tracers with higher specific activity. It also has the advantage of not requiring any valves, but the disadvantage of requiring larger chip real estate.

With any of these approaches, it is possible to concentrate a significant fraction of the radioactivity from a cyclotron bombardment into a volume that can be loaded onto the microfluidic chip, enabling radiochemistry to be performed in microliter volumes with high radioactivity.

7.3.3 Synthesis Automation

As with radiosynthesis in conventional systems at milliliter volume scales, it is important that the apparatus is operated in an automated fashion within radiation shielding to ensure the safety of the operator preparing the PET tracer. Fully automated synthesizers have been developed based on some of the earlier reports of batch microfluidic chips, complete with reagent delivery, radioisotope concentration, synthesis, and cartridge-based purification or interfacing with an HPLC system [15, 17, 50, 56].

For the more recent EWOD microfluidic platform, many aspects of automating the overall system have been demonstrated. Two approaches have been developed for loading reagents from off-chip reservoirs (e.g., standard septum-capped glass reagent vials) into the chip. One simple approach uses an electronically controlled syringe pump to precisely dispense the desired volume of reagent after compensating for evaporation losses at the dispensing tip [57]. Another approach was developed in collaboration with Sofie Biosciences, Inc. to avoid the use of complex, difficult-to-clean components such as syringe pumps and valves, instead of relying on simple disposable fluidic elements such as needles and tubing. Inert gas pressure and gravitational force were used to apply forward and reverse driving forces, respectively, to deliver repeatable volumes to the chip [58]. A multi-reagent loading interface was developed based on this principle and was integrated with a simple cartridge-based method for upstream [^{18}F]fluoride concentration and an automated method for downstream collection of the crude product from the chip and interfacing with miniature solid-phase extraction cartridges or analytical-scale HPLC for purification [34]. Some preliminary progress to develop methods for on-chip purification has also been made including removal of unreacted [^{18}F]fluoride

using an alumina surface [35] or beads [36], and more complete separation may be possible by performing on-chip solid-phase extraction. A prototype of a complete EWOD-based PET tracer production system suitable for benchtop operation is under development at Sofie Biosciences in collaboration with our group.

7.4 Conclusions and Outlook

The development of batch microfluidic devices may provide an ideal platform to harness the numerous advantages of performing the synthesis of PET radiotracers in small volumes, including reduced reagent consumption, improved specific activity, reduced radiolysis, and synthesizer miniaturization. In particular, the EWOD platform is compatible with diverse reaction conditions and provides a convenient means to digitally manipulate droplets to perform diverse multistep reactions. By combining these devices with technologies for concentration of radioisotopes into an automated platform, it will become possible to produce not only batches on demand for research use but even large-scale batches in a radiopharmacy for distribution purposes. This microvolume radiochemistry technique could also be a particularly good match for isotopic exchange and biomolecule labeling reactions and could enable novel chemistries by boosting [^{18}F]fluoride concentration by orders of magnitude. As a tool for remotely and safely handling small volumes, the EWOD microfluidic platform could open up opportunities for researchers to uncover additional benefits of radiochemistry in extremely small volumes.

Acknowledgments The authors gratefully acknowledge support for writing this review from the National Institute of Biomedical Imaging and Bioengineering (grant R21EB015540), the National Institute on Aging (grant R21AG049918), as well as Sofie Biosciences, Inc., and the National Institute of Mental Health (grant R44MH097271).

References

1. Phelps ME. Positron emission tomography provides molecular imaging of biological processes. PNAS. 2000;97:9226–33.
2. Kelloff GJ, Hoffman JM, Johnson B, et al. Progress and promise of FDG-PET imaging for cancer patient management and oncologic drug development. Clin Cancer Res. 2005;11:2785–808.

3. Lasne M-C, Perrio C, Rouden J, Barré L, Roeda D, Dolle F, Crouzel C. Chemistry of β+−emitting compounds based on fluorine-18. In: Krause W, editor. Contrast agents II. Berlin/Heidelberg: Springer; 2002. p. 201–58.
4. Keng PY, Esterby M, van Dam RM. Emerging technologies for decentralized production of PET tracers. In: Hsieh C-H, editor. Positron emission tomography – current clinical and research aspects. InTech; 2012. p. 153–82.
5. Rensch C, Jackson A, Lindner S, Salvamoser R, Samper V, Riese S, Bartenstein P, Wängler C, Wängler B. Microfluidics: a groundbreaking technology for PET tracer production? Molecules. 2013;18:7930–56.
6. Miller PW, deMello AJ, Gee AD. Application of microfluidics to the ultra-rapid preparation of fluorine-18 labelled compounds. Curr Radiopharm. 2010;3:254–62.
7. Watts P, Pascali G, Salvadori PA. Positron emission tomography radiosynthesis in microreactors. J Flow Chem. 2012;2:37–42.
8. McMullen JP, Jensen KF. Integrated microreactors for reaction automation: new approaches to reaction development. Annu Rev Anal Chem. 2010;3:19–42.
9. Gillies JM, Prenant C, Chimon GN, Smethurst GJ, Perrie W, Hamblett I, Dekker B, Zweit J. Microfluidic reactor for the radiosynthesis of PET radiotracers. Appl Radiat Isot. 2006;64:325–32.
10. Steel CJ, O'Brien AT, Luthra SK, Brady F. Automated PET radiosyntheses using microfluidic devices. J Label Compd Radiopharm. 2007;50:308–11.
11. Wester H-J, Schoultz BW, Hultsch C, Henriksen G. Fast and repetitive in-capillary production of [18F]FDG. Eur J Nucl Med Mol Imaging. 2009;36:653–8.
12. Pascali G, Watts P, Salvadori PA. Microfluidics in radiopharmaceutical chemistry. Nucl Med Biol. 2013;40:776–87.
13. Rensch C, Lindner S, Salvamoser R, et al. A solvent resistant lab-on-chip platform for radiochemistry applications. Lab Chip. 2014;14:2556–64.
14. Arima V, Pascali G, Lade O, et al. Radiochemistry on chip: towards dose-on-demand synthesis of PET radiopharmaceuticals. Lab Chip. 2013;13(12):2328–36.
15. Lee C-C, Sui G, Elizarov A, et al. Multistep synthesis of a radiolabeled imaging probe using integrated microfluidics. Science. 2005;310:1793–6.
16. Elizarov AM, van Dam RM, Shin YS, Kolb HC, Padgett HC, Stout D, Shu J, Huang J, Daridon A, Heath JR. Design and optimization of coin-shaped microreactor chips for PET radiopharmaceutical synthesis. J Nucl Med. 2010;51:282–7.
17. Tseng W-Y, Cho JS, Ma X, Kunihiro A, Chatziioannou A, van Dam RM. Toward reliable synthesis of radiotracers for positron emission tomography in PDMS microfluidic chips: study and optimization of the [18F] fluoride drying process. In: Technical proceedings of the 2010 NSTI nanotechnology conference and trade show, Anaheim, CA. Boca Raton: CRC Press; 2010. p. 472–5.
18. Lebedev A, Miraghaie R, Kotta K, Ball CE, Zhang J, Buchsbaum MS, Kolb HC, Elizarov A. Batch-reactor microfluidic device: first human use of a microfluidically produced PET radiotracer. Lab Chip. 2012;13:136–45.
19. Liu K, Lepin EJ, Wang M-W, et al. Microfluidic-based 18F-labeling of biomolecules for immuno-positron emission tomography. Mol Imaging. 2011;10:168–76.
20. Zeng D, Desai AV, Ranganathan D, Wheeler TD, Kenis PJA, Reichert DE. Microfluidic radiolabeling of biomolecules with PET radiometals. Nucl Med Biol. 2013;40:42–51.
21. Keng PY, Chen S, Ding H, et al. Micro-chemical synthesis of molecular probes on an electronic microfluidic device. PNAS. 2012;109:690–5.
22. Reichert DE. A digital revolution in radiosynthesis. J Nucl Med. 2014;55:181–2.
23. Sadeghi S, Ding H, Shah GJ, Chen S, Keng PY, Kim C-J "CJ", van Dam RM, On chip droplet characterization: a practical, high-sensitivity measurement of droplet impedance in digital microfluidics. Anal Chem. 2012;84:1915–23.
24. Javed MR, Chen S, Kim H-K, Wei L, Czernin J, Kim C-J "CJ," Dam RM van, Keng PY. Efficient radiosynthesis of 3′-deoxy-3′-18F-fluorothymidine using electrowetting-on-dielectric digital microfluidic chip. J Nucl Med. 2014;55:321–8.

25. Javed MR, Chen S, Lei J, Collins J, Sergeev M, Kim H-K, Kim C-J, van Dam RM, Keng PY. High yield and high specific activity synthesis of [18F]fallypride in a batch microfluidic reactor for micro-PET imaging. Chem Commun. 2014;50:1192–4.
26. Chen S, Javed MR, Kim H-K, Lei J, Lazari M, Shah GJ, van Dam M, Keng PY, Kim C-J. Radiolabelling diverse positron emission tomography (PET) tracers using a single digital microfluidic reactor chip. Lab Chip. 2014;14:902–10.
27. Koag MC, Kim H-K, Kim AS. Efficient microscale synthesis of [18F]-2-fluoro-2-deoxy-d-glucose. Chem Eng J. 2014;258:62–8.
28. Koag MC, Kim H-K, Kim AS. Fast and efficient microscale radiosynthesis of 3′-deoxy-3′-[18F]fluorothymidine. J Fluor Chem. 2014;166:104–9.
29. Fawdry RM. Radiolysis of 2-[18F]fluoro-2-deoxy-d-glucose (FDG) and the role of reductant stabilisers. Appl Radiat Isot. 2007;65:1193–201.
30. Búriová E, Macášek F, Melichar F, Kropáček M, Procházka L. Autoradiolysis of the 2-deoxy-2-[18F]fluoro-D-glucose radiopharmaceutical. J Radioanal Nucl Chem. 2005;264:595–602.
31. Jacobson MS, Dankwart HR, Mahoney DW. Radiolysis of 2-[18F]fluoro-2-deoxy-d-glucose ([18F]FDG) and the role of ethanol and radioactive concentration. Appl Radiat Isot. 2009;67:990–5.
32. Levin CS, Hoffman EJ. Calculation of positron range and its effect on the fundamental limit of positron emission tomography system spatial resolution. Phys Med Biol. 1999;44:781.
33. Rensch C, Waengler B, Yaroshenko A, Samper V, Baller M, Heumesser N, Ulin J, Riese S, Reischl G. Microfluidic reactor geometries for radiolysis reduction in radiopharmaceuticals. Appl Radiat Isot. 2012;70:1691–7.
34. Lazari M, Collins J, Shen B, Farhoud M, Yeh D, Maraglia B, Chin FT, Nathanson DA, Moore M, van Dam RM. Fully automated production of diverse 18F-labeled PET tracers on the ELIXYS multireactor radiosynthesizer without hardware modification. J Nucl Med Technol. 2014;42:203–10.
35. Shah GJ, Lei J, Chen S, Kim C-J "CJ," Keng PY, Van Dam RM. Automated injection from EWOD digital microfluidic chip into HPLC purification system. In: Proceedings of the 16th international conference on miniaturized systems for chemistry and life sciences, Okinawa. London: Royal Society of Chemistry; 2012. p. 356–8.
36. Chen S, Lei J, van Dam RM, Keng P-Y, Kim C-J "CJ". Planar alumina purification of 18F-labeled radiotracer synthesis on EWOD chip for positron emission tomography (PET). In: Proceedings of the 16th international conference on miniaturized systems for chemistry and life sciences, Okinawa. London: Royal Society of Chemistry; 2012. p. 1771–3.
37. Chen S, Dooraghi A, Lazari M, van Dam RM, Chatziioannou A, Kim C-J. On-chip product purification for complete microfluidic radiotracer synthesis. In: Proceedings of the 27th IEEE international conference on micro electro mechanical systems (MEMS), San Francisco, CA. Piscataway: IEEE; 2014. p. 284–7.
38. Tarn MD, Pascali G, De Leonardis F, Watts P, Salvadori PA, Pamme N. Purification of 2-[18F] fluoro-2-deoxy-d-glucose by on-chip solid-phase extraction. J Chromatogr A. 2013;1280:117–21.
39. Hume SP, Gunn RN, Jones T. Pharmacological constraints associated with positron emission tomographic scanning of small laboratory animals. Eur J Nucl Med Mol Imaging. 1998;25:173–6.
40. Lapi SE, Welch MJ. A historical perspective on the specific activity of radiopharmaceuticals: What have we learned in the 35 years of the ISRC? Nucl Med Biol. 2013;40:314–20.
41. Satyamurthy N, Amarasekera B, Alvord CW, Barrio JR, Phelps ME. Tantalum [18O]water target for the production of [18F]fluoride with high reactivity for the preparation of 2-deoxy-2-[18F]fluoro-D-glucose. Mol Imaging Biol. 2002;4:65–70.
42. Solin O, Bergman J, Haaparanta M, Reissell A. Production of 18F from water targets. Specific radioactivity and anionic contaminants. Int J Radiat Applications and Instrumentation Part A Applied Radiation and Isotopes. 1988;39:1065–71.

43. Füchtner F, Preusche S, Mäding P, Zessin J, Steinbach J. Factors affecting the specific activity of [18F]fluoride from a [18O]water target. Nuklearmedizin. 2008;47:116–9.
44. Berridge MS, Apana SM, Hersh JM. Teflon radiolysis as the major source of carrier in fluorine-18. J Label Compd Radiopharm. 2009;52:543–8.
45. Lazari M, Sergeev M, Liu Z, Perrin DM, van Dam RM. Study of specific activity in isotopic exchange radiofluorination performed on a microfluidic device. Seoul: World Molecular Imaging Congress; 2014.
46. Sergeev M, Lazari M, Collins J, Morgia F, Javed MR, Keng PY, van Dam RM. Investigation of effect of reaction volume on specific activity in macro- and microscale fluorine-18 radiosynthesis. In: Proceedings of the 6th international symposium on microchemistry and microsystems (ISMM), Singapore; 2014. p. 77–8.
47. Ting R, Lo J, Adam MJ, Ruth TJ, Perrin DM. Capturing aqueous [18F]-fluoride with an arylboronic ester for PET: synthesis and aqueous stability of a fluorescent [18F]-labeled aryltrifluoroborate. J Fluor Chem. 2008;129:349–58.
48. Liu Z, Li Y, Lozada J, Pan J, Lin K-S, Schaffer P, Perrin DM. Rapid, one-step, high yielding 18F-labeling of an aryltrifluoroborate bioconjugate by isotope exchange at very high specific activity. J Label Compd Radiopharm. 2012;55:491–6.
49. Nelson WC, Kim JY. Monolithic fabrication of EWOD chips for picoliter droplets. J Microelectromech Syst. 2011;20:1419–27.
50. Lazari M, Narayanam MK, Murphy JM, Van Dam MR. Automated concentration of 18F-fluoride into microliter volumes. In: 21st international symposium on radiopharmaceutical sciences, Columbia, MO; 2015.
51. Bejot R, Elizarov AM, Ball E, Zhang J, Miraghaie R, Kolb HC, Gouverneur V. Batch-mode microfluidic radiosynthesis of N-succinimidyl-4-[18F]fluorobenzoate for protein labelling. J Label Compd Radiopharm. 2011;54:117–22.
52. Ismail R, Irribarren J, Javed MR, Machness A, van Dam M, Keng PY. Cationic imidazolium polymer monoliths for efficient solvent exchange, activation and fluorination on a continuous flow system. RSC Adv. 2014;4:25348–56.
53. De Leonardis F, Pascali G, Salvadori PA, Watts P, Pamme N. On-chip pre-concentration and complexation of [18F]fluoride ions via regenerable anion exchange particles for radiochemical synthesis of positron emission tomography tracers. J Chromatogr A. 2011;1218:4714–9.
54. Sadeghi S, Liang V, Cheung S, Woo S, Wu C, Ly J, Deng Y, Eddings M, van Dam RM. Reusable electrochemical cell for rapid separation of [18F]fluoride from [18O]water for flow-through synthesis of 18F-labeled tracers. Appl Radiat Isot. 2013;75:85–94.
55. Saiki H, Iwata R, Nakanishi H, Wong R, Ishikawa Y, Furumoto S, Yamahara R, Sakamoto K, Ozeki E. Electrochemical concentration of no-carrier-added [18F]fluoride from [18O]water in a disposable microfluidic cell for radiosynthesis of 18F-labeled radiopharmaceuticals. Appl Radiat Isot. 2010;68:1703–8.
56. Lu S, Giamis AM, Pike VW. Synthesis of [18F]fallypride in a micro-reactor: rapid optimization and multiple-production in small doses for micro-PET studies. Curr Radiopharm. 2009;2:1–13.
57. Van Dam RM, Elizarov AM, Ball CE, et al. Automated microfluidic-chip-based stand-alone instrument for the synthesis of radiopharmaceuticals on human-dose scales. In: Technical proceedings of the 2007 NSTI nanotechnology conference and trade show, Santa Clara, CA. Boca Raton: CRC Press; 2007. p. 300–3.
58. Ding H, Sadeghi S, Shah GJ, Chen S, Keng PY, Kim CJ, van Dam M. Accurate dispensing of volatile reagents on demand for chemical reactions in EWOD chips. Lab Chip. 2012;12:3331–40.
59. Shah GJ, Ding H, Sadeghi S, Chen S, Kim C-J, van Dam RM. Milliliter-to-microliter platform for on-demand loading of aqueous and non-aqueous droplets to digital microfluidics. In: Proceedings of the 16th international solid-state sensors, actuators and microsystems conference (TRANSDUCERS), Beijing. Piscataway: IEEE; 2011. p. 1260–3.

60. Chen Y-C, Liu K, Shen CK-F, van Dam RM. On-demand generation and mixing of liquid-in-gas slugs with digitally programmable composition and size. J Micromech Microeng. 2015;25:084006.
61. Wheeler AR, Moon H, Kim C-J, Loo JA, Garrell RL. Electrowetting-based microfluidics for analysis of peptides and proteins by matrix-assisted laser desorption/ionization mass spectrometry. Anal Chem. 2004;76:4833–8.
62. Cho SK, Moon H, Kim C-J. Creating, transporting, cutting, and merging liquid droplets by electrowetting-based actuation for digital microfluidic circuits. J MEMS. 2003;12:70–80.
63. Barbulovic-Nad I, Yang H, Park P, Wheeler A. Digital microfluidics for cell-based assays. Lab Chip. 2008;8:519.

Chapter 8
Development of a Microreactor for Synthesis of ^{18}F-Labeled Positron Emission Tomography Probe

Norihito Kuno, Naomi Manri, Norifumi Abo, Yukako Asano, Ken-ichi Nishijima, Nagara Tamaki, and Yuji Kuge

Abstract *Background*: The application of microreactors to positron emission tomography (PET) probe radiosynthesis has attracted a great deal of interest because of its potential to increase specific activity and yields of probes and to reduce reaction time, expensive regent consumption, and the footprint of the device/instrument. To develop a microreactor platform that enables the synthesis of various ^{18}F-labeled PET probes, a prototype microreactor with a novel "split-flow and interflow mixing" (split mixing) was fabricated and applied to ^{18}F-labeling reactions.

Methods: The split mixing microreactor, made of Al_2O_3 resistant to several solvents, had higher mixing performance than that of the conventional batch

N. Kuno (✉)
Center for Exploratory Research, Research and Development Group, Hitachi, Ltd., 1-280, Higashi-koigakubo, Kokubunji, Tokyo 185-8601, Japan
e-mail: norihito.kuno.py@hitachi.com

N. Manri
Center for Technology Innovation – Healthcare, Research and Development Group, Hitachi, Ltd., 1-280, Higashi-koigakubo, Kokubunji, Tokyo 185-8601, Japan
e-mail: naomi.manri.hd@hitachi.com

N. Abo • K. Nishijima
Central Institute of Isotope Science, Hokkaido University, Kita 15 Nishi 7, Kita-ku, Sapporo 060-0815, Japan
e-mail: abo@ric.hokudai.ac.jp; nishijim@ric.hokudai.ac.jp

Y. Asano
Center for Technology Innovation – Mechanical Systems, Research and Development Group, Hitachi, Ltd., 832-2 Horiguchi, Hitachinaka, Ibaraki 312-0034, Tokyo, Japan
e-mail: yukako.asano.dp@hitachi.com

N. Tamaki
Department of Nuclear Medicine, Graduate School of Medicine, Hokkaido University, Sapporo, Japan
e-mail: natamaki@med.hokudai.ac.jp

Y. Kuge
Central Institute of Isotope Science, Hokkaido University Department of Integrated Molecular Imaging, Graduate School of Medicine, Hokkaido University, Sapporo, Japan
e-mail: kuge@ric.hokudai.ac.jp

Y. Kuge et al. (eds.), *Perspectives on Nuclear Medicine for Molecular Diagnosis and Integrated Therapy*, DOI 10.1007/978-4-431-55894-1_8

method. Two ^{18}F-labeling reactions (^{18}F labeling of bovine serum albumin (BSA) by N-succinimidyl-4-[^{18}F] fluorobenzoate (SFB) and 1-(2′-nitro-1′-imidazolyl)-2-O-tetrahydropyranyl-3-O-toluenesulfonylpropanediol (NITTP) by ^{18}F) were conducted using the microreactor.

Results: The ^{18}F-labeling yield of BSA obtained by using the microreactor was almost the same as that by using the conventional batch method; however, the reaction time of the microreactor was slightly shorter than that of the batch method. Conversely, the ^{18}F-labeling yield of NITTP obtained by using the microreactor was about half that by using the batch method. The low NITTP-labeling yield was due to adsorption of naked ^{18}F to the surface of micro-mixing channel in the microreactor. The prescreening of candidate materials with lower ^{18}F adsorption for the microreactor was carried out with solvent resistance and solvent absorption as indexes. As a result of this prescreening, cyclo olefin polymer (COP) was selected as a candidate. A prototype COP microreactor has been fabricated and is being evaluated in terms of ^{18}F labeling.

Conclusions: Although the higher mixing performance of the split mixing microreactor did not significantly contribute to increasing ^{18}F-labeling yield, it did contribute to shortening reaction time. Moreover, the material used for the microreactor should be carefully selected from the viewpoint of developing a microreactor platform that enables the synthesis of various ^{18}F-labeled PET probes.

Keywords Positron emission tomography (PET) • Microreactor • ^{18}F-labeled PET probe • Cyclo olefin polymer (COP)

8.1 Introduction

Positron emission tomography (PET) is a noninvasive, nuclear imaging technique that has been widely applied for medical research and clinical diagnosis in the fields of oncology, neurology, and cardiology [1–4]. PET imaging relies on the utilization of a PET probe labeled with short-lived positron-emitting radioisotopes such as ^{11}C (t1/2 = 20 min) or ^{18}F (t1/2 = 110 min). Among several PET probes, 2-^{18}F-fluoro-2-deoxy-d-glucose (^{18}F-FDG), an analog of glucose, is most commonly used in the diagnosis and assessment of cancer. Moreover, utilized in clinical oncology, it shows excellent performance as a PET imaging probe [5].

^{18}F-FDG has been extensively utilized as the PET imaging probe in oncologic application. However, in the last few decades, a large number of non-FDG PET probes have been developed to measure and elucidate various biological and physiological processes [6, 7].

With the Increasing variation of PET probes that are applicable to clinical diagnosis, for diagnosis of individual patients, it is necessary to produce a wide variety of PET probes in small quantities. It is therefore also necessary to modify the supply system for PET probe (such as a centralized mass production) and the commercial delivery system that were established for a single PET probe, i.e., ^{18}F-FDG [8].

Meanwhile, decentralized, in-house production of PET probes also has some difficulties in regard to the production of a wide variety of PET probes in small quantities, because of the need for a large investment in infrastructure in accordance with government regulations, an expensive "hot cell" for radiation shielding of PET probe synthesizer, and high personnel and operating costs. Moreover, the number of synthesizer that can be installed in a hot cell is restricted because of the limited workspace in the hot cell; accordingly, it is difficult to accomplish in-house small-scale production of multiple PET probes.

Recently, to solve the abovementioned problems concerning small-scale production of various PET probes, the application of microreactors (or microfluidic devices) to the PET probe radiosynthesis has attracted a great deal of interest because of their potential to increase specific activity and yields of the probes and to reduce reaction time, consumption of expensive reagents, and footprint of the device/instrument [9, 10].

Microreactor can be categorized as flow-through type or batch type. And both a flow-through microreactor and a batch microreactor have been applied to radiosynthesis of PET probes for ^{18}F labeling [11]. Almost all previous studies on applying microreactors for radiosynthesis of PET probes have been limited to preclinical PET imaging; however, a few recent studies attempted to apply microreactors for synthesizing the clinical PET probes such as ^{18}F-fallypride, the dopamine D2/D3 receptors imaging probe [12]; 7-(6-fluoropyridin-3-yl)-5H-pyrido [4,3-b]indole (^{18}F-T807), tau imaging probe [13]; and ^{18}F-labeled 3-fluoro-5-[(pyridin-3-yl)ethynyl]benzonitrile (^{18}F-FPEB), the glutamate receptor subtype type 5 (mGluR5) imaging probe [14].

Moreover, a microreactor for radiosynthesis of a clinical PET probe has not been applied as the routine production method for clinical usage. It is still a great challenge to solve several problems hindering the practical use of microreactors for synthesizing PET imaging probes for clinical applications.

In a previous study, microreactor systems with novel mixing methods were established and applied to achieve large-scale and industrial production of chemicals [15, 16]. In this study, a prototype microreactor with a novel split-flow and interflow mixing (called "split mixing") was fabricated and evaluated in regard to ^{18}F-labeling reactions.

8.2 Materials and Methods

8.2.1 Villermaux-Dushman Method

The mixing performance of the prototype microreactor was evaluated by Villermaux-Dushman method [17]. Solution X (HCl: 0.1374 M) and solution Y (KI, 0.01595 M; CH_3COONa, 1.33 M; KIO_3, 0.003175 M) were separately supplied to the microreactor by Micro Process Server (MPS-α200, Hitachi, Tokyo,

Japan). The solution mixed in the microreactor was collected and left for two minutes. The flow rate of the two solutions was set at 0.2, 0.5, 1.0, 2.0, 4.0, and 6.0 mL/min. Absorbance at 350 nm was measured by a UV-visible spectrometer (U-3010, Hitachi-High Technologies, Tokyo, Japan).

8.2.2 ^{18}F Labeling of BSA by ^{18}F-SFB

Succinimidyl-4-[^{18}F]fluorobenzoate (^{18}F-SFB) was synthesized by a method similar to that reported by Tang et al. [18]. The synthesized ^{18}F-SFB was evaporated at 100 °C under an argon stream and dissolved in 20 % acetonitrile (MeCN) (0.3 MBq/μL). Bovine serum albumin (BSA) dissolved in 125 mM borate buffer (pH8.8) (5 mg/mL) was used as a target protein. By the microreactor method, ^{18}F-SFB and BSA solutions were separately injected into the microreactor by using the MPS-α200. The mixed solution was introduced into a PTFE tube (φ0.17 × 250 mm, GL science, Tokyo, Japan) connected to an outlet of the microreactor. The reaction mixture was collected at times of 2, 10, and 20 min by driving the MPS-α200, and TFA was added to the reaction mixture to terminate the reaction. By the conventional batch method, the ^{18}F-SFB and BSA solutions were mixed in equal amount at room temperature in a 1.5 mL microtube. Trifluoroacetic acid (TFA) was added to the mixture to terminate the reaction at times of 2, 10, and 20 min.

LC analysis was performed using a Nexera X2 UHPLC/HPLC system (Shimadzu, Kyoto, Japan). The reaction mixture (20 μL) was loaded onto a C8 reversed-phase column (CAPCELL PAK C8 SG300, Shiseido, Tokyo, Japan). The LC solvents were (A) 2 % MeCN/0.05 % TFA and (B) 80 % MeCN/0.05 % TFA, and a gradient (40 % B: 0–1.5 min, 100 % B: 1.5–2.5 min, 40 % B: 2.5–9.0 min) was used at a flow rate of 0.3 mL/min. The percentage of ^{18}F-benzoic acid (^{18}F-FBzA),^{18}F-SFB, and ^{18}F-BSA was calculated from the LC data.

8.2.3 ^{18}F Labeling of NITTP by ^{18}F

An aqueous solution of $^{18}F^-$, produced by cyclotron using the ^{18}O (p, n) ^{18}F reaction, was passed through a Sep-Pak Light QMA cartridge (Waters Corporation, MA, USA). The ^{18}F activity was eluted with a 0.9 mL (0.7 mL MeCN/0.2 mL water) solution containing 14 mg Kryptofix222 (K222) and 1.4 mg K_2CO_3. The eluent was then evaporated at 100 °C under an argon stream. The residue, containing $[K/K222]^{+18}F^-$, was dissolved in dimethyl sulfoxide (DMSO) (0.22 MBq/μL).

1-(2′-Nitro-1′-imidazolyl)-2-O-tetrahydropyranyl-3-O-toluenesulfonyl-propanediol (NITTP, ABX GmbH, Radeberg, Germany) was dissolved in DMSO (1.3 mg/mL). By the microreactor method, $[K/K222]^{+18}F^-$ and NITTP solutions

were separately sent to the microreactor by using a dual syringe pump (TSP-202, YMC, Kyoto, Japan). The solution mixed in the microreactor was then sent to a PTFE tube (φ0.5 × 510 mm, GL science) connected to an outlet of the microreactor, and the reaction in the PTFE tube was allowed to proceed for 3 or 10 min at 80 °C. By the batch method, $[K/K222]^{+}{}^{18}F^{-}$ and NITTP solutions were mixed in equal amount in a 1.5 mL microtube. The reaction was allowed to proceed for 3 or 10 min at 80 °C. LC analysis was performed using a Nexera X2 (Shimadzu). The reaction mixture (10 μL) was loaded onto a C18 reversed-phase column (XBridge C18, 5 μm, 4.6 mm × 150 mm, Waters Corporation). The LC solvents were (A) 50 mM $(NH_4)_2HPO_4$ and (B) MeCN, and isocratic elution (45 % B) was used at a flow rate of 1 mL/min. Percentage of ^{18}F-NITTP was calculated from the LC data.

8.2.4 Solvent Resistance Test

The chemical resistance of seven materials (polyvinyl chloride [PVC], polystyrene [PS], acrylonitrile-butadiene-styrene resin [ABS], methacrylate resin [PMMA], polycarbonate [PC], polypropylene [PP], and cyclo olefin polymer [COP]) against five chemicals (acetonitrile [MeCN], dimethyl sulfoxide [DMSO], hydrochlonic [HCl], sodium hydroxide [NaOH], and ethanol [EtOH]) was tested. A test piece (size: 10 × 10 × t2 mm) was dropped into each of the chemicals set at 25, 50, 80, or 120 °C, and the reaction was allowed to proceed for 30 min. The condition of the test piece was observed, and the weight of the test piece was measured (W1) after the reaction was completed. After the test piece was washed with water, it was dehydrated for 24 h at 50 °C. The weight of the test piece was measured again (W2). The volume of the chemical absorbed in the test piece was calculated from the difference between W1 and W2.

8.3 Results and Discussion

8.3.1 Microreactor with Novel Mixing System

Two microreactors with different types of mixing, i.e., split-flow and interflow ("split mixing") and multilayer channels contracting toward the downstream ("multimixing"), were fabricated (Fig. 8.1a, b). The split mixing microreactor was made of Al_2O_3, and the multimixing one was made of PEEK. Both materials, Al_2O_3 and PEEK, were selected from the viewpoint of resistance to several solvents and fabricability of micro channel structure for mixing.

On the split mixing microreactor, the first liquid (solution A) and the second liquid (solution B) were injected into the micro channels of the microreactor. The

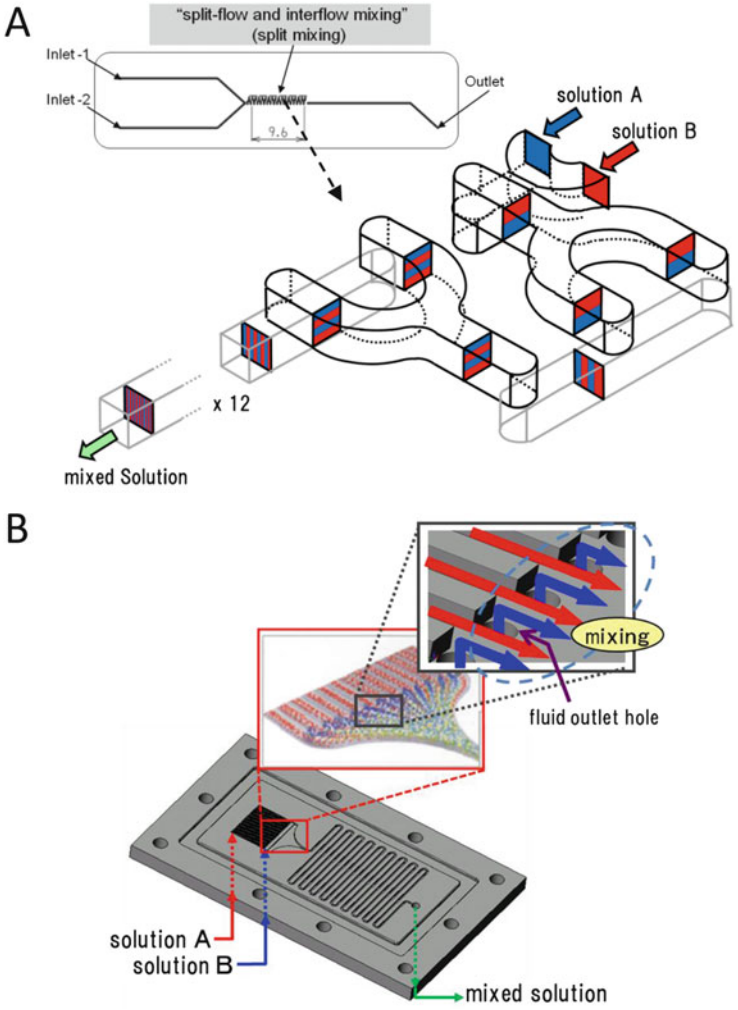

Fig. 8.1 Schematics of microreactors used in this study. (**a**) The split-flow and interflow microreactor. The flow of fluids in the micro channel for mixing is shown in the cross section of the micro channel. (**b**) The multilayer channels contracting toward the downstream microreactor

parallel flow of two fluids (solutions A and B) was split, rotated 90° (inversion), and interflowed repeatedly (12 times) as the fluids pass through the repeated split mixing structures of the microreactor. Finally, the flow of two fluids formed an alternately multilayered thin flow of fluids (Fig. 8.1a). As the thickness of each fluid became small, the diffusion time of the reactants of fluids (solutions A and B) was reduced, causing faster mixing of the solutions.

On the multimixing microreactor, the first liquid (solution A) flows from each nozzle in layer form on top of the chip. In the center of the chip, the second liquid

(solution B) supplied from multi-outlet holes flows into the layered first liquid. Then, both fluids form a multilayered flow at a contraction flow part on the bottom of the chip to produce the thin flow of fluids (Fig. 8.1b).

8.3.2 *Evaluation of Mixing Performance of Prototype Microreactors*

Mixing performance of the prototype microreactors was evaluated by using the Villermaux-Dushman method [17], shown in Fig. 8.2a. By this method, the side reaction product, I_3^-, was spectroscopically measured by using the mean of UV absorbance at 350 nm. Therefore, lower UV absorbance indicates higher mixing performance. The mixing performance of the split mixing microreactor was higher than that of the multimixing microreactor and that of a conventional batch method (Fig. 8.2b). From this result, the split mixing microreactor was selected for further analysis of ^{18}F-labeling reaction.

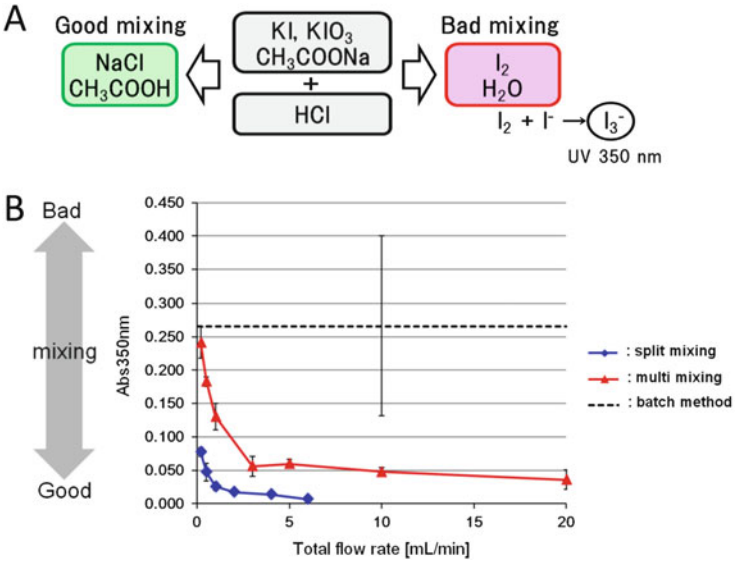

Fig. 8.2 (**a**) Schematic of the Villermaux-Dushman method. (**b**) Mixing performance of the split-flow and interflow ("split mixing") microreactor (◇) and the multilayer channels contracting toward the downstream ("multimixing") microreactor (△)

8.3.3 *^{18}F Labeling of Bovine Serum Albumin (BSA) by N-succinimidyl-4-^{18}F Fluorobenzoate (^{18}F-SFB)*

The ^{18}F-labeling reaction of BSA by ^{18}F-SFB was examined to evaluate the ^{18}F-labeling performance of the split mixing microreactor. This reaction consists of a main reaction (^{18}F labeling of BSA) and a side reaction which produce ^{18}F-fluorobenzoic acid (^{18}F-FBzA) as a by-product (Fig. 8.3a).

As shown in Fig. 8.3b, the ^{18}F-labeling yield of BSA obtained by using the split mixing microreactor was almost the same as that by using the conventional batch method (Fig. 8.3b). A by-product, ^{18}F-FBzA, was synthesized in the same manner as that of batch method. These results suggest that as well as the main reaction, the side reaction is likely to proceed due to the higher mixing performance of the split mixing-type microreactor; therefore, the higher mixing performance might not be effective for increasing the ^{18}F-labeling yield of BSA.

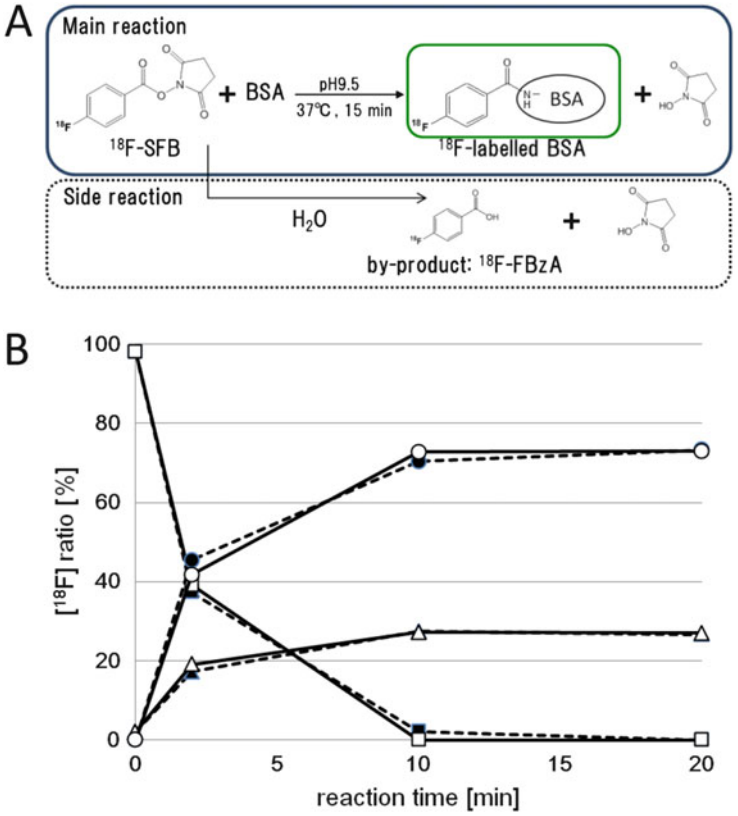

Fig. 8.3 (**a**) Synthesis of ^{18}F-labeled BSA by N-succinimidyl-4-^{18}F fluorobenzoate (^{18}F-SFB). (**b**) Time courses of ^{18}F-BSA (○, ●), ^{18}F-FBzA (△, ▲), and ^{18}F-SFB (◇, ◆) synthesis of the split mixing microreactor (*solid line*) and the conventional batch method (*broken line*)

The reaction time of ^{18}F labeling of BSA was estimated from a reaction rate constant calculated from the HPLC data. The estimated reaction time (10 min) for the ^{18}F labeling of BSA by the microreactor method was shorter than that by the batch method (12 min). This result suggests that high mixing performance contributes to shortening the reaction time.

8.3.4 *^{18}F Labeling of 1-(2′-nitro-1′-imidazolyl)-2-O-tetrahydropyranyl-3-O-toluenesulfonylpropanediol (NITTP) by ^{18}F*

To further evaluate the ^{18}F-labeling performance of the split mixing microreactor, the ^{18}F-labeling reaction of NITTP was investigated (Fig. 8.4a). NITTP is a precursor for the synthesis of ^{18}F-fluoromisonidazole (^{18}F-FMISO), which is a PET imaging probe for determining the tumor hypoxia in vivo [19].

The ^{18}F-labeling yield of NITTP (at reaction time of 10 min) obtained by using the microreactor was 26 %, which is about half of that by using the batch method (59 %) (Fig. 8.4b). By measuring the total ^{18}F activity of all solutions applied for the microreactor reaction, only 65 % of the initial ^{18}F activity was recovered, and about 20 % of that was remained in the micro channels of microreactor. This result suggests that the low NITTP-labeling yield is due to adsorption of naked ^{18}F to the

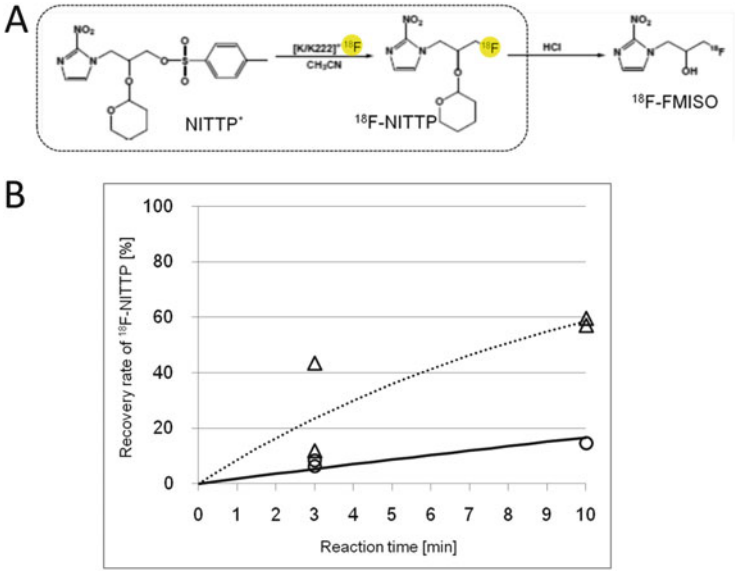

Fig. 8.4 (**a**) Synthesis of ^{18}F-NITTP and ^{18}F-FMISO. (**b**) Time courses of ^{18}F-NITTP synthesis of the split mixing microreactor (○, *solid line*) and the conventional batch method (△, *broken line*)

surface of micro channels. To improve the ^{18}F-labeling yield of NITTP attained by naked ^{18}F, the material used for the microreactor should be reexamined.

8.3.5 *Screening of Material for the Split Mixing Microreactor*

As a first step of selecting the material for the microreactor, prescreening of candidate materials was carried out with solvent resistance and solvent absorption as indexes. The solvent resistance and absorption of seven kinds of materials, namely, polyvinyl chloride (PVC), polystyrene (PS), acrylonitrile-butadiene-styrene resin (ABS), methacrylate resin (PMMA), polycarbonate (PC), polypropylene (PP), and cyclo olefin polymer (COP), were tested for acetonitrile (MeCN), dimethyl sulfoxide (DMSO), hydrochloric acid (HCl), sodium hydroxide (NaOH), and ethanol (EtOH) at 25, 50, and 80 °C. Among these materials, PP and COP exhibited relatively better solvent resistant and lower solvent absorption than other materials. PP and COP exhibited excellent solvent resistant and lower absorption for HCl, NaOH, and EtOH; however, at the higher temperature, PP showed a decrease of solvent resistant and COP showed little absorption of solvent (Table 8.1).

As a candidate material for the microreactor, COP was selected for the microreactor because of the higher solvent resistance at high temperature (80 °C) of COP. As a preliminary experiment, a prototype COP microreactor was fabricated, and the remaining ^{18}F activity after passing a ^{18}F containing solution through the micro channels of the COP microreactor was determined. The remaining ^{18}F activity was about 5 % of total ^{18}F activity injected into the microreactor, which is lower than that (35 %) in the case of Al_2O_3 microreactor. This result indicates that the COP microreactor is applicable to efficient ^{18}F labeling for PET imaging probe.

Table 8.1 Solvent resistance and absorption test

		MeCN			DMSO		
	Temp (°C)	25	50	80	25	50	80
PP	Resistance	+	+	−	+	+	+
	Absorption(μl)	<5	<5	5 ~ 10	<5	<5	<5
COP	Resistance	+	+	+	+	+	+
	Absorption(μl)	<5	<5	<5	<5	5 ~ 10	5 ~ 10

+, resistance; −, nonresistance

8.4 Conclusion

Although the higher mixing performance of the microreactor did not significantly contribute to increasing the ^{18}F-labeling yield, it did contribute to shortening the reaction time. Moreover, selecting the appropriate material for the microreactor is crucial from the viewpoint of developing a microreactor platform that enables the synthesis of various ^{18}F-labeled PET probes.

Acknowledgment This work was supported in part by the Creation of Innovation Centers for Advanced Interdisciplinary Research Areas Program, Ministry of Education, Culture, Sports, Science and Technology, Japan.

References

1. Phelps ME. Positron emission tomography provides molecular imaging of biological processes. Proc Natl Acad Sci U S A. 2000;97:9226–33.
2. Gambhir SS. Molecular imaging of cancer with positron emission tomography. Nat Rev Cancer. 2002;2:683–93.
3. Politis M, Piccini P. Positron emission tomography imaging in neurological disorders. J Neurol. 2012;259:1769–80.
4. Schindler TH, Schelbert HR, Quercioli A, Dilsizian V. Cardiac PET imaging for the detection and monitoring of coronary artery disease and microvascular health. JACC Cardiovasc Imaging. 2010;3:623–40.
5. Otsuka H, Graham M, Kubo A, Nishitani H. Clinical utility of FDG PET. J Med Invest. 2004;51:14–9.
6. Brower V. Beyond FDG: many molecular imaging agents are in development. J Natl Cancer Inst. 2011;103:13–5.
7. The Radiosynthesis Database of PET Probes (RaDaP). National Institute of Radiological Sciences, Japan. 2013. http://www.nirs.go.jp/research/division/mic/db2/
8. Keng PY, Esterby M, van Dam RM. Emerging technologies for decentralized production of PET tracers. In: Hsieh CH, editor. Positron emission tomography – current clinical and research aspects. Rijeka: InTech; 2012. p. 53–182.
9. Lu SY, Pike VW. Micro-reactors for PET tracer labeling. In: Schubiger PA, Lehmann L, Friebe M, editors. PET chemistry. Berlin: Springer; 2007. p. 271–87.
10. Pascali G, Watts P, Salvadori PA. Microfluidics in radiopharmaceutical chemistry. Nucl Med Biol. 2013;40:776–87.
11. Elizarov AM. Microreactors for radiopharmaceutical synthesis. Lab Chip. 2009;9:1326–33.

12. Lebedev A, Miraghaie R, Kotta K, Ball CE, Zhang J, Buchsbaum MS, Kolb HC, Elizarov A. Batch-reactor microfluidic device: first human use of a microfluidically produced PET radiotracer. Lab Chip. 2013;13:136–45.
13. Liang SH, Yokell DL, Normandin MD, Rice PA, Jackson RN, Shoup TM, Brady TJ, El Fakhri G, Collier TL, Vasdev N. First human use of a radiopharmaceutical prepared by continuous-flow microfluidic radiofluorination: proof of concept with the tau imaging agent [^{18}F]T807. Mol Imaging 2014;13. doi:10.2310/7290.2014.00025.
14. Liang SH, Yokell DL, Jackson RN, Rice PA, Callahan R, Johnson KA, Alagille D, Tamagnan G, Collier TL, Vasdev N. Microfluidic continuous-flow radiosynthesis of [^{18}F] FPEB suitable for human PET imaging. Medchemcomm. 2014;5:432–5.
15. Asano Y, Togashi S, Tsudome H, Murakami S. Microreactor technology: innovations in production processes. Pharm Eng. 2010;8:32–42.
16. Asano Y, Miyamoto T, Togashi S, Endo Y. Study on the sandmeyer reaction via an unstable diazonium ion in microreactors with reaction rate analyses. J Chem Eng Jpn. 2014;47:287–95.
17. Ehrfeld W, Golbig K, Hessel V, Löwe H, Richter T. Characterization of mixing in micromixers by a test reaction: single mixing units and mixer arrays. Ind Eng Chem Res. 1999;38:1075–82.
18. Tang G, Zeng W, Yu M, Kabalka G. Facile synthesis of N-succinimidyl 4-[^{18}F]fluorobenzoate ([^{18}F]SFB) for protein labeling. J Label Compd Radiopharm. 2008;51:68–71.
19. Dubois L, Landuyt W, Haustermans K, Dupont P, Bormans G, Vermaelen P, Flamen P, Verbeken E, Mortelmans L. Evaluation of hypoxia in an experimental rat tumour model by [(18)F] fluoromisonidazole PET and immunohistochemistry. Br J Cancer. 2004;91:1947–54.

Chapter 9
Preclinical Evaluation of a Thymidine Phosphorylase Imaging Probe, [^{123}I]IIMU, for Translational Research

Ken-ichi Nishijima, Songji Zhao, Fei Feng, Yoichi Shimizu, Hiromichi Akizawa, Kazue Ohkura, Nagara Tamaki, and Yuji Kuge

Abstract The expression of thymidine phosphorylase (TP) is closely associated with angiogenesis, tumor invasiveness, and activation of antitumor agents. We developed a radiolabeled uracil derivative, I-123-labeled 5-iodo-6-[(2-iminoimidazolidinyl)methyl]uracil ([^{123}I]IIMU), as a novel SPECT probe for TP. A clinical study to verify the safety of [^{123}I]IIMU injection was approved by the Institutional Review Board of Hokkaido University Hospital for Clinical Research, and first-in-human (FIH) clinical studies of healthy adults were started.

Here, we will introduce our research, including the synthesis of [^{123}I]IIMU and its efficacy and safety evaluation, toward its FIH clinical study.

Radiosynthesis of [^{123}I]IIMU: [^{123}I]IIMU synthesis was achieved by radioiodination of the precursor, 6-(2-iminoimidazolidinyl)methyluracil at the

K. Nishijima
Central Institute of Isotope Science, Hokkaido University, Sapporo, Japan

Graduate School of Medicine, Hokkaido University, Sapporo, Japan

S. Zhao • F. Feng
Graduate School of Medicine, Hokkaido University, Sapporo, Japan

Y. Shimizu
Faculty of Pharmaceutical Sciences, Hokkaido University, Sapporo, Japan

H. Akizawa
Showa Pharmaceutical University, Machida, Japan

K. Ohkura
Faculty of Pharmaceutical Sciences, Health Sciences University of Hokkaido, Sapporo, Japan

N. Tamaki
Department of Nuclear Medicine, Graduate School of Medicine, Hokkaido University, Sapporo, Japan

Y. Kuge (✉)
Central Institute of Isotope Science, Hokkaido University Department of Integrated Molecular Imaging, Graduate School of Medicine, Hokkaido University, Sapporo, Japan
e-mail: kuge@ric.hokudai.ac.jp

Y. Kuge et al. (eds.), *Perspectives on Nuclear Medicine for Molecular Diagnosis and Integrated Therapy*, DOI 10.1007/978-4-431-55894-1_9

C-5 position with *N*-chlorosuccinimide/[^{123}I]NaI. After purification by HPLC, [^{123}I]IIMU was obtained in high radiochemical yields.

In vitro and in vivo *studies*: The in vitro and in vivo uptake of [^{125}I]IIMU by the A431 tumor was attributable to the binding of the radiotracer to its target enzyme, i.e., TP. SPECT/CT imaging with [^{123}I]IIMU clearly visualized the A431 tumor 3 h after the injection of n.c.a. [^{123}I]IIMU.

Safety *assessment*: The human radiation absorbed dose was estimated as 17 μSv/MBq on the basis of the biodistribution data of [I]IIMU in normal mice. The no observed adverse effect level (NOAEL) for intravenous administration of non-radiolabeled IIMU to mice was higher than 1.8 mg/kg. The bacterial reverse mutation assay showed negative results.

Keywords Thymidine • Phosphorylase • SPECT

9.1 Introduction

Thymidine phosphorylase (TP) catalyzes the reversible phosphorolysis of thymidine to thymine and 2-deoxyribose-1-phosphate. The expression of TP is highly associated with angiogenesis, infiltration, and metastasis of tumors. The activity and expression level of TP in many tumors are higher than those in the adjacent nonneoplastic tissues [1].

We developed a radiolabeled uracil derivative, I-123-labeled 5-iodo-6-[(2-iminoimidazolidinyl)methyl]uracil ([^{123}I]IIMU, Fig. 9.1), as a novel SPECT probe for TP. A clinical study to verify the safety of [^{123}I]IIMU injection was approved by the Institutional Review Board of Hokkaido University Hospital for Clinical Research, and first-in-human (FIH) clinical studies on healthy adults were started.

Here, we will introduce our research, including the synthesis of [^{123}I]IIMU [2, 3] and its efficacy [4–6] and safety evaluation, toward its FIH clinical study.

9.2 Radiosynthesis of [^{123}I]IIMU [2]

[^{123}I]IIMU was synthesized according to a method previously reported [3]. Briefly, dry acetone containing *N*-chlorosuccinimide/AcOH was added to [^{123}I]NaI (370 MBq) in a reaction vial, and the mixture was allowed to stand for 10 min at room temperature. Acetone was then removed completely under a stream of N_2. A

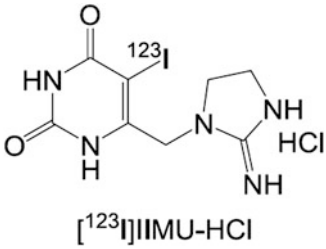

Fig. 9.1 Structure of [^{123}I] IIMU hydrochloride

Table 9.1 Production data for three consecutive syntheses of [^{123}I]IIMU

	Run number			
Parameter	1	2	3	Mean ± SD
Yield at the end of preparation (MBq)	232	189	193	205 ± 24
Radiochemical yield (%)	62	51	52	55 ± 6
Radiochemical purity (%)	>99	>99	>99	>99

Table 9.2 Results of quality control tests for three consecutive syntheses of [^{123}I]IIMU

		Run number			
Parameter		1	2	3	Mean ± SD
pH		7	7	7	7 ± 0
Residual organic solvent (ppm)	EtOH	46.8	232.6	33.4	104 ± 111
	MeCN	2.2	ND	2.3	1.5 ± 1.3
	Acetone	ND	ND	ND	–
Tests for bacterial endotoxins		Negative	Negative	Negative	–
Sterility test		Negative	Negative	Negative	–
ND: Not detected (<1.0)					

solution of 6-[(2-iminoimidazolidinyl)methyl]uracil (HIMU-TFA) in aqueous acetonitrile ($CH_3CN/H_2O = 2:1$) was added to the residue, and the capped vial was heated for 35 min at 50 °C. After removal of the solvent, the crude product was converted to [^{123}I]IIMU-HCl and purified simultaneously by reversed-phase HPLC using a solvent system containing HCl. The radioactive fraction was sterilized through a 0.22 μm membrane filter. The radiochemical purity of [^{123}I]IIMU was determined with HPLC. Residual organic solvents were determined with GC. Sterility tests and bacterial endotoxin tests were also performed.

[^{123}I]IIMU for intravenous injection was prepared in 2.5 h with a yield of 205 ± 24 MBq ($n = 3$). The radiochemical purity of [^{123}I]IIMU was found to be more than 99 % (Table 9.1). The results of the quality control tests are summarized in Table 9.2. Acetone was not detected in the solution. The ethanol concentration was 104 ± 111 ppm. Sterility tests and bacterial endotoxin tests showed negative results (Table 9.2). We successfully prepared [^{123}I]IIMU for intravenous injection with high purity. Results of quality control tests demonstrate that the [^{123}I]IIMU preparation is suitable for clinical studies.

9.3 In Vitro *Study*: Uptake of [^{125}I]IIMU in Cultured A431 and AZ521 Cells [4]

Immunoblotting for the detection of TP demonstrated high enzyme expression in A431 human epithelial carcinoma cells and very low expression in AZ521 human gastric cancer cells. A431 or AZ521 cells in 24-well plates were incubated at 37 °C in 1 mL of PBS(−) containing 37 kBq of [^{125}I]IIMU for 10, 30, 60, or 120 min. The

incubation solution was removed, and cells were washed and solubilized in 0.7 mL of 0.2 M NaOH. The radioactivity and protein content of the cell lysate were evaluated. When the radiotracer was incubated with A431 cells, the uptake level of the radiotracer increased with an increase in the incubation time, with 5.3 % dose/mg protein at 2 h of incubation. In the case of AZ521 cells, uptake of radioactivity was extremely low, 0.68 % dose/mg protein at most, regardless of incubation time. To confirm whether the observed uptake is due to the binding of the tracer to TP, similar experiments with A431 tumors were conducted in the presence of various concentrations of nonlabeled IIMU. The uptake level of [^{125}I]IIMU in A431 cells was reduced depending on the concentration of nonlabeled IIMU.

9.4 In Vivo *Study*: Biodistribution of [^{125}I]IIMU in A431 and AZ521 Tumor-Bearing Nude Mice [4]

The entire experimental protocol was approved by the Laboratory Animal Care and Use Committee of Hokkaido University. A saline solution of [^{125}I]IIMU (37 kBq, 0.1 mL) was injected into the tail vein of A431 or AZ521 tumor-bearing female Balb/cAJc1-nu/nu mice (8 weeks old; about 20 g). At 0.5, 1, 3, and 24 h after administration, animals were euthanized and the organs of interest and blood were collected. Radioactivity levels in the blood and muscle were similar in A431 and AZ521 tumor-bearing mice. However, tumor accumulation levels were markedly different between the two; the A431 tumor with high TP expression showed high accumulation, while AZ521 tumor with low TP expression showed low accumulation. To hamper the binding of the tracer to TP, an excess amount of non-radiolabeled IIMU was administered to A431 tumor-bearing mice and the biodistribution was evaluated at 0.5 h postinjection. The radioactivity in A431 tumor was reduced by co-injection of nonlabeled IIMU.

The in vitro and in vivo uptake of [^{125}I]IIMU by the A431 tumor was attributable to the binding of the radiotracer to its target enzyme, i.e., TP.

9.5 SPECT/CT Imaging Study [2]

Small-animal SPECT imaging studies were performed in mice bearing A431 xenografts after intravenous injection of non-carrier-added (n.c.a.) [^{123}I]IIMU or [^{123}I]IIMU with an excessively large amount of nonlabeled IIMU ($n = 3$ per group) by using a small-animal PET/SPECT/CT. SPECT/CT imaging with [^{123}I]IIMU clearly visualized A431 tumor 3 h after the injection of n.c.a. [^{123}I]IIMU (Fig. 9.2a). The accumulation of [^{123}I]IIMU in the tumor and liver was inhibited by the co-injection of non-radiolabeled IIMU (Fig. 9.2b).

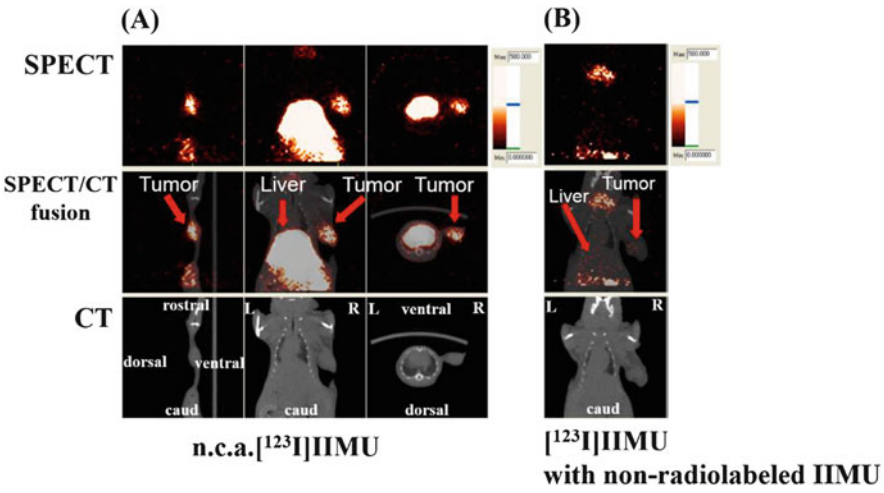

Fig. 9.2 SPECT/CT images of mice bearing A431 tumors. Mice were injected with 25 MBq of n.c.a. [^{123}I]IIMU (**a**) or [^{123}I]IIMU with non-radiolabeled IIMU (**b**)

9.6 Safety Assessment

To realize the application of [^{123}I]IIMU to clinical studies, we performed safety assessment of [^{123}I]IIMU. Evaluation of radiation absorbed dose is important for the safety assessment of radiopharmaceuticals. The human radiation absorbed dose was estimated as 17 μSv/MBq on the basis of the biodistribution data of [^{125}I]IIMU in normal mice. The highest radiation dose was of the urinary bladder (130 μGy/MBq), followed by the liver (75.1 μGy/MBq), thyroid (47.3 μGy/MBq), and gallbladder (20.4 μGy/MBq). The human radiation absorbed dose of [^{123}I]IIMU was considered to be within the allowable range and is equal to or less than the human radiation absorbed dose of [^{18}F]FDG (21 μSv/MBq; ICPR 60).

Also, based on the "guidance for conducting microdose clinical trials," we performed an extended single-dose toxicity study and the bacterial reverse mutation assay (Ames test). In the extended single-dose toxicity study, SD rats were given a single intravenous dose (0, 0.18, and 1.8 mg/kg) on Day 1, followed by observations until termination on Day 14. There were no deaths or in-life clinical signs and there were no microscopic effects. The no observed adverse effect level (NOAEL) for intravenous administration of nonlabeled IIMU to mice was greater than 1.8 mg/kg. The bacterial reverse mutation assay showed negative results.

9.7 Conclusions

Our findings indicate that [^{123}I]IIMU should be developed as a diagnostic agent for imaging TP-expressing tumors. It was shown that [^{123}I]IIMU injection can be safely administered in preclinical studies. Examinations using [^{123}I]IIMU for injection are expected to provide useful information that is difficult to obtain by other conventional methods, such as estimation/determination of therapeutic effects of anticancer drugs, decision-making for a treatment plan, prognostic prediction, understanding of disease stages, and malignancy assessment.

References

1. Takebayashi Y, Yamada K, Miyadera K, et al. The activity and expression of thymidine phosphorylase in human solid tumors. Eur J Cancer. 1996;32A:1227–32.
2. Nishijima K, Zhao S, Zhao Y, et al. Preparation and evaluation of [^{123}I]IIMU for SPECT imaging of thymidine phosphorylase expression in tumors. J Label Compd Radiopharm. 2013;56:S1–S349.
3. Takahashi M, Seki K, Nishijima K, et al. Synthesis of a radioiodinated thymidine phosphorylase inhibitor and its preliminary evaluation as a potential SPECT tracer for angiogenic enzyme expression. J Label Compd Radiopharm. 2008;51:384–7.
4. Akizawa H, Zhao S, Takahashi M, et al. In vitro and in vivo evaluations of a radioiodinated thymidine phosphorylase inhibitor as a tumor diagnostic agent for angiogenic enzyme imaging. Nucl Med Biol. 2010;37:427–32.
5. Li H, Zhao S, Jin Y, et al. Radiolabeled uracil derivative as a novel SPECT probe for thymidine phosphorylase: suppressed accumulation into tumor cells by target gene knockdown. Nucl Med Commun. 2011;32:1211–5.
6. Zhao S, Li H, Nishijima K et al. Relationship between biodistribution of a novel thymidine phosphorylase (TP) imaging probe and TP expression levels in normal mice. Ann Nucl Med. 2015;29:582-7.

Chapter 10
Discovery and Evaluation of Biomarkers for Atherosclerosis

Differential Proteomics of Plasma and Tissues

Takeshi Sakamoto, Hiroko Hanzawa, Naomi Manri, Mamoru Sakakibara, Yoichi Shimizu, Yan Zhao, Songji Zhao, Shiro Yamada, Kiwamu Kamiya, Yutaka Eki, Akihiro Suzuki, Haruhiko Higuchi, Chiaki Sugano, Hiroyuki Tsutsui, Nagara Tamaki, and Yuji Kuge

Abstract The usage of biomarkers reflecting atherosclerosis progression is important for preventing serious incidence of cardiovascular events. To elucidate clinically relevant molecular determinants in atherosclerosis, we have taken a comprehensive approach to combine mass spectrometry-based differential proteomics using both clinical and animal model specimens. Clinical plasma samples were collected from patients with acute myocardial infarction (AMI), stable angina (SA), and healthy/low-risk individuals (H-LR). We also obtained plasma and arterial tissue samples from apolipoprotein E-deficient and wild-type mice at various pathognomonic points of age. Cleavable isotope-coded affinity tags were

T. Sakamoto (✉)
Research & Development Group, Hitachi, Ltd., 1-280, Higashi-koigakubo, Kokubunji, Tokyo 185-8601, Japan

Department of Nuclear Medicine, Graduate School of Medicine, Hokkaido University, Sapporo 060-8638, Japan
e-mail: takeshi.sakamoto.yg@hitachi.com

H. Hanzawa • N. Manri
Research & Development Group, Hitachi, Ltd., 1-280, Higashi-koigakubo, Kokubunji, Tokyo 185-8601, Japan

Central Institute of Isotope Science, Hokkaido University, Sapporo 060-0814, Japan

M. Sakakibara • S. Yamada • K. Kamiya • H. Tsutsui
Department of Cardiovascular Medicine, Graduate School of Medicine, Hokkaido University, Sapporo 060-8638, Japan

Y. Shimizu
Laboratory of Bioanalysis and Molecular Imaging, Faculty of Pharmaceutical Sciences, Hokkaido University, Sapporo 060-0812, Japan

Y. Zhao • N. Tamaki
Department of Nuclear Medicine, Graduate School of Medicine, Hokkaido University, Sapporo 060-8638, Japan

Y. Kuge et al. (eds.), *Perspectives on Nuclear Medicine for Molecular Diagnosis and Integrated Therapy*, DOI 10.1007/978-4-431-55894-1_10

used for differential mass spectrometry. Differential proteomics of clinical plasma samples revealed that more than 10 proteins appeared to be upregulated (relative abundance AMI/H-LR or SA/H-LR >1.5) and 5 proteins downregulated (AMI/H-LR or SA/H-LR <1/1.5). These trends associated with the disease progression are not always coincident with those of mouse ortholog proteins, suggesting a pathophysiological difference between humans and the mouse model. Among the downregulated proteins, the complement factor D (CFD) showed monotonic decrease that was in good agreement with the enzyme-linked immunosorbent assay. These results suggest that the comprehensive and systematic proteomic approach may be promising in terms of the selection and evaluation of biomarker candidates.

Keywords Proteomic study • Atherosclerosis • Inflammation • apoE-deficient mouse

10.1 Introduction

Atherosclerosis is a chronic inflammatory disease and often causes subsequent thrombotic complication. It is well known as a main etiology of critical diseases such as acute coronary syndrome including myocardial infarction, sudden cardiac death, and stroke [1]. To detect the signs of severe incidences, it is important to accurately evaluate the progression stages of atherosclerosis, vulnerability, and rupture risk of atherosclerotic plaques. Therefore, a variety of approaches to establish novel biomarkers directly reflecting the status of atherosclerosis have been conducted to date [2]. However, due to the complexity of the disease, discovery and clinical validation of such biomarkers are still underway in many institutions.

S. Zhao
Department of Tracer Kinetics & Bioanalysis, Graduate School of Medicine, Hokkaido University, Sapporo 060-8638, Japan

Y. Eki • A. Suzuki • H. Higuchi
Hitachi General Hospital, Hitachi, Ltd., Hitachi 317-0077, Japan

C. Sugano
Hitachinaka General Hospital, Hitachi, Ltd., Hitachinaka 312-0057, Japan

Y. Kuge
Central Institute of Isotope Science, Hokkaido University Department of Integrated Molecular Imaging, Graduate School of Medicine, Hokkaido University, Sapporo, Japan

Disease proteomics is a profiling technology using mass spectrometry that makes it possible to identify disease-related alteration of protein expression comprehensively in a wide variety of biological specimens including serum or plasma or extracts from tissues of interests [3]. Numerous studies have been conducted to develop biomarkers for early diagnosis, selection of appropriate therapy, and prognosis assessment. A decade of progress to determine changes in disease-related protein expression has achieved accurate and high-throughput quantification of the individual proteins within mixtures by using differential stable isotopic labeling, such as cleavable isotope-coded affinity tags (cICATs) [4]. Either light or heavy cICATs are labeled at the free thiol groups of cysteine residues of which proteins are isolated from two distinct samples (i.e., disease and healthy states). The ratio of protein amount between these states is estimated by comparing MS signal intensity of the corresponding proteolytic peptide fragments [4].

To elucidate clinically relevant molecular determinants in atherosclerotic development, we have taken a comprehensive approach by using mass spectrometry-based differential proteomics. First, we conducted differential human plasma proteomic studies using clinical samples of patients with atherosclerosis-related cardiovascular disease and healthy (or low-risk) volunteers. Second, to validate the results we obtained in the studies, a biomarker candidate, the complement factor D (CFD) level of patients with atherosclerosis-related cardiovascular disease, was determined by carrying out an enzyme-linked immunosorbent assay (ELISA). Then, we tried combining differential proteome of plasma and arterial tissue obtained from both wild-type (WT) and apoED mice at four pathognomonic time points of age. Finally, we compared identified proteins in humans with mouse plasma proteome.

10.2 Materials and Methods

This study was approved by the Ethics Committee of Hokkaido University Hospital (no. 010–0118) and the institutional ethics committees of Hitachi, Ltd. Clinical plasma samples were collected prospectively for 48 acute myocardial infarction (AMI) patients, 73 stable angina (SA) patients, and 69 healthy/low-risk (H-LR) individuals.

Animal care and animal experiments were conducted at Japan SLC, Inc. (Hamamatsu, Japan), under the approval of the company's animal care committee. The apoED (C57BL/6.KOR/StmSlc-Apoeshl) and WT (C57BL/6) mice were fed a high-fat diet from 8 weeks of age. Plasma and arterial tissues were collected from each group of male or female mice at ages of 12, 18, 25, and 35 weeks.

Proteins prepared from plasma or arterial tissue as described above were labeled with isotope-coded affinity tags using the Cleavable ICAT® Reagent Kit (Applied Biosystems, Foster City, USA) according to the manufacturer's instructions with minor modifications. Tryptic peptides were applied to the strong cation exchange (SCX) column, and the eluted solution was fractionated into 25 fractions. The SCX separated fractions were analyzed using NanoFrontier LD, a liquid chromatograph

mass spectrometry (LC-MS) system (Hitachi High-Technologies Corporation, Tokyo, Japan). Original MS/MS peak lists (PLs) were generated using built-in PL generation software in the mass spectrometer, and further protein/peptide identification and cICAT quantitative analyses were conducted using a custom developed software platform with a relational database.

Plasma CFD levels were measured with the use of ELISA kits according to the manufacturer's instructions (Quantikine, DFD00, R&D Systems, Inc., Minneapolis, USA). Plasma levels of known markers including high-sensitive C-reactive protein (hsCRP), amino-terminal pro-brain natriuretic peptide (NT-pro BNP), and adiponectin were also determined (SRL, Inc., Tokyo, Japan).

10.3 Results and Discussion

Atherosclerosis is a chronic inflammatory disease, in which atherosclerotic lesions are formed in blood vessels through complicated molecular processes occurring between the circulating blood stream and lesions. To identify proteins showing changes in expression levels associated with atherosclerotic plaque progression, we

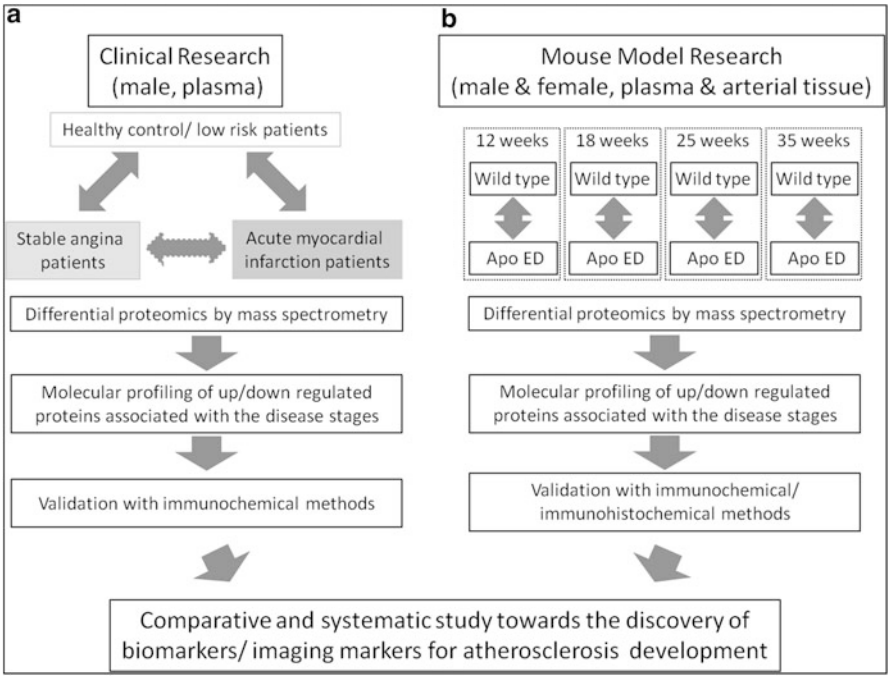

Fig. 10.1 Entire research workflow of stage-dependent, mass spectrometry-based differential proteomics. (**a**) Clinical proteomic study using human plasma samples. (**b**) Animal model proteomic study using plasma and arterial tissue samples from WT and atherosclerotic model mice

conducted mass spectrometry-based proteomic analyses. Figure 10.1 shows an overall picture of the proteomic experiments we have done. Most previous proteomic studies have focused on only one point of the disease. However, these strategies would not be adequate to indentify proteins showing serial quantitative change in accordance with progression of atherosclerosis. In this study, we conducted a differential proteome study at several characteristic points of disease stage and compared the results of identified proteins. The proteins we identified that showed changes in plasma level according to the severity of the atherosclerosis-related disease (e.g., ischemic heart disease) or atherosclerosis progression of the mouse model might be diagnostic or predictive biomarker candidates for blood testing. On the other hand, the proteins that showed changes, especially an increase tendency, in arterial tissues might be biomarkers for diagnostic imaging.

10.3.1 Disease Stage-Dependent Differential Proteome in Human Plasma

As shown in Fig. 10.1, we conducted disease stage-dependent differential human plasma proteomic experiments using clinical samples. We selected three clinical conditions, H-LR, SA, and AMI (Table 10.1). Two independent age-matched plasma pools from each group ($n = 7$) were used for the experiments with combinations of H-LR vs. SA, H-LR vs. AMI, and SA vs. AMI. Table 10.2 shows the summary of identified proteins by differential proteomics of clinical plasma samples. We identified about 110 proteins in each trial of differential proteome and found that 8–13 proteins appeared to be upregulated (relative abundance AMI/H-LR or SA/H-LR >1.5), and 2–8 proteins were downregulated (AMI/H-LR or SA/H-LR $<1/1.5$). Finally, five identical proteins were identified in common between trials 1 and 2. Three were blood coagulation related, such as von Willebrand factor, and the other two were categorized as structural-integrity-related or immunoresponse (immunoglobulin)-related proteins. The downregulated proteins identified in common between trials were found to be apolipoproteins involving cholesterol homeostasis, blood coagulation, and CFD.

To validate the results we obtained in the differential proteome experiments as described above, we determined the CFD level of plasma of clinical samples by ELISA as a representative example. We found that CFD levels in plasma of the AMI group were the lowest among the three clinical groups. The statistical

Table 10.1 Description of three clinical groups in human plasma proteome

Description	H-LR	SA	AMI
Group	Healthy and low-risk volunteers	Patients with stable angina	Patients with acute myocardial infarction
Risk and progression stage of atherosclerosis	Low	Moderate/early	High/advanced

Table 10.2 Up- or downregulated proteins detected by differential proteomic analysis in clinical pooled plasma samples

Group		SA/H-LR	AMI/H-LR	AMI/SA
Total number of identified proteins	Trial 1	116	115	110
	Trial 2	106	112	114
Upregulated	Trial 1	8	8	5
	Trial 2	7	8	13
	Common	1	5	2
Downregulated	Trial 1	4	6	8
	Trial 2	7	2	5
	Common	2	1	1

H-LR group of healthy control and low-risk volunteers, *SA* group of patients with stable angina, *AMI* group of patients with acute myocardial infarction, *Upregulated* proteins showed expression ratio >1.5, *Downregulated* proteins showed expression ratio <1/1.5

difference of AMI to H-LR was the most pronounced (H/LR vs. AMI, $p = 2.4 \times 10^{-10}$; H/LR vs. SA, $p = 0.54$). The diminished plasma levels of CFD in AMI patients showed that the results we obtained in our proteomic study were basically verified. Furthermore, the plasma CFD levels showed no correlation with body mass index (BMI) ($r = 0.03$, $P < 0.05$), hsCRP ($r = -0.09$, $P < 0.05$), NT-proBNP ($r = -0.03$, $P < 0.05$), and adiponectin ($r = 0.11$, $P < 0.05$). In recent years, it has been suggested that the activation of the complement system plays a role in atherosclerosis progression [5]. Among the components of the complement pathway, CFD is known as a key regulatory serine protease of the alternative complement pathway. CFD mRNA and protein are abundantly expressed in adipose tissue, and the protein is found at high levels in serum [6]. CFD expression levels in rodent models of obesity are reduced [7]. Our results may suggest some kind of CFD implication in atherosclerosis.

10.3.2 Disease Stage-Dependent Differential Proteome in Atherosclerosis Mouse Model

As shown in Fig. 10.1, we conducted differential proteome experiments using plasma and arterial tissues of WT and apolipoprotein E-deficient (apoED) mice. Table 10.3 shows phenotypic characteristics of atherosclerotic lesions of WT and apoED at each point of age. As we previously demonstrated, on a high-fat diet, early lesions were observed in apoED at 12–18 weeks of age, and advanced lesions were prominent at 25–35 weeks. No atherosclerotic lesions were found in WT mice throughout four points of age [8]. At 25 weeks of age, vulnerable atheromatous lesions were more abundant, but fibroatheromatous lesions were less at 25 weeks than those at 35 weeks [8]. Table 10.4 shows a summary of identified proteins. In plasma, the total number of identified proteins and the ratio of their upregulated

Table 10.3 Description of possible progression stages of atherosclerotic lesion of atherosclerosis mouse model

Age (weeks)		12	18	25	35
Risk and progression stage of atherosclerosis	WT	None	None	None	None
	apoED	Low/early	Low/early	High/ advanced	Moderate/ advanced
Lesion phenotype	WT	None	None	None	None
	apoED	Monocyte adhesion	Foam cell formation	Vulnerable plaque	Stable plaque

Table 10.4 Summary of up- or downregulated proteins detected in plasma and arterial tissues by differential proteome of mouse model

	Plasma				Arterial tissue			
Age (weeks)	12	18	25	35	12	18	25	35
Total number of identified proteins	146	133	119	124	446	616	659	693
Upregulated (%)	7	14	15	11	8	6	16	16
Downregulated (%)	5	5	11	15	2	5	8	9
No change (%)	88	81	74	74	90	89	76	75

Upregulated expression ratio (apoED/WT) >1.5, *Downregulated* expression ratio (apoED/WT) $<$ 1/1.5, *No change* $1/1.5 <$ expression ratio (apoED/WT) < 1.5. This table is modified from reference [9]

proteins (expression ratio, apoED/WT; > 1.5) did not significantly change throughout the time course (Table 10.4). However, the ratio of downregulated proteins (apoED/WT; $<1/1.5$) increased on and after 25 weeks of age (Table 10.4). We finally found 100 proteins in the plasma, and 390 proteins in the arterial tissues were detected throughout all four time points: 29 were identified in common between plasma and arterial tissues [data not shown, 9]. Interestingly, we found that disease stage-dependent quantitative variation patterns did not always correspond between plasma and arterial tissues. Furthermore, proteins showed characteristic change in abundance in plasma, and/or arterial tissues were found to be components of inflammation, thrombus formation, and vascular remodeling [9].

10.3.3 Comparison Between Human and Mouse Plasma Proteome

In this study, we conducted disease stage-dependent differential proteome experiments in two identical studies: one for human plasma proteome using clinical samples and one for plasma/arterial tissue proteome using an atherosclerotic mouse model, apoED. Importantly, we found that the changes associated with the disease progression in the amount of identified proteins were not always coincident

with those of mouse ortholog proteins in plasma or arterial tissues determined by proteomic studies (data not shown). In case of CFD, the plasma level of CFD in humans determined in the proteomic study or ELISA decreased in accordance with the severity of the clinical conditions. On the other hand, the plasma level of CFD in mice showed a slight but not significant decreasing tendency determined in differential proteome between WT mice and the apoED mouse model. We preliminarily determined the plasma level of CFD in mice by ELISA and detected no statistical significance between WT mice and apoED throughout all four time points. CD5L, a soluble member of the scavenger receptor cysteine-rich domain superfamily protein, did not show any significant change in abundance as determined by human plasma differential analyses. However, the expression ratios (apoED/WT) of CD5L in mouse plasma were high throughout the four time points [9]. In addition, we found that CD5L accumulated in advanced lesions of apoED in accordance with macrophage infiltration by immunohistochemistry. These results suggest that fundamental mechanisms of atherosclerosis development are similar to each other; however, there would be a pathophysiological difference between humans and the mouse model.

10.3.4 Limitation

We failed to detect several known atherosclerotic plaque-related proteins such as cytokines, monocyte chemoattractant protein-1 (MCP-1), and intercellular adhesion molecule-1(ICAM-1). We assume that there were several technical reasons for this. For example, the practical detection limit in our mass spectrometry system was assumed to be 1–10 ng/mL, which is much higher than the normal concentration of cytokines. We used cICAT labeling reagents, which covalently bind only to cysteine residues of targeted proteins. Therefore, it becomes difficult to detect proteins with trypsin-digested peptides with few or no cysteine residues.

10.4 Conclusion

To identify proteins showing changes in expression levels associated with atherosclerotic plaque progression, we conducted mass spectrometry-based proteomic analyses. We adopted two separate study designs: one for human plasma differential proteome using clinical samples and one for mouse plasma/arterial tissue differential proteome using samples obtained from wild-type mice and an atherosclerotic mouse model apoED. Then several proteins showing quantitative changes in accordance with disease were found, including the complement factor D (CFD). The diminished plasma levels of CFD in acute myocardial infarction patients were verified in an enzyme-linked immunosorbent assay. These results suggest that CFD might be a potential biomarker for atherosclerosis. The comprehensive and

systematic proteomic approach using different states of samples is promising in terms of the selection of biomarker candidates.

Acknowledgments This study was supported in part by the grant "The matching program for innovations in future drug discovery and medical care" from the Ministry of Education, Culture, Sports, Science, and Technology, Japan (to Tamaki, N.). The authors thank Megumi Hikichi, Yuko Komori, and Yumi Yanagiya for their technical assistance. Without their help and support, we could never have done this study.

References

1. Ross R. Atherosclerosis – an inflammatory disease. N Engl J Med. 1999;340:115–26.
2. Wang X, Connolly TM. Biomarkers of vulnerable atheromatous plaques: translational medicine perspectives. Adv Clin Chem. 2010;50:1–22.
3. Hanash S. Disease proteomics. Nature. 2003;422:226–32.
4. Gygi SP, Rist B, Gerber SA, et al. Quantitative analysis of complex protein mixtures using isotope-coded affinity tags. Nat Biotechnol. 1999;17:994–9.
5. Torzewski M, Bhakdi S. Complement and atherosclerosis-united to the point of no return? Clin Biochem. 2013;46:20–5.
6. Cook KS, Min HY, Jonson D, et al. Adipsin: a circulating serine protease homolog secreted by adipose tissue and sciatic nerve. Science. 1987;237:402–5.
7. Flier JS, Cook KS, Usher P, et al. Severely impaired adipsin expression in genetic and acquired obesity. Science. 1987;237:405–8.
8. Zhao Y, Kuge Y, Zhao S, et al. Prolonged high-fat feeding enhances aortic ^{18}F-FDG and ^{99m}Tc-Annexin A5 uptake in apolipoprotein E-deficient and wild-type C57BL/6J Mice. J Nucl Med. 2008;49:1707–14.
9. Hanzawa H, Sakamoto T, Kaneko A, et al. Combined plasma and tissue proteomic study of atherogenic model mouse: Approach to elucidate molecular determinants in atherosclerosis development. J Proteome Res. 2015;14:4257–69.

Chapter 11
Radioimmunodetection of Atherosclerotic Lesions Focusing on the Accumulation Mechanism of Immunoglobulin G

Yoichi Shimizu, Hiroko Hanzawa, Yan Zhao, Ken-ichi Nishijima, Sagiri Fukura, Takeshi Sakamoto, Songji Zhao, Nagara Tamaki, and Yuji Kuge

Abstract In the diagnosis of atherosclerosis, detailed evaluation of biomarkers related to its lesion formation is desired for estimation of its progression rate. In our previous proteomic studies of atherosclerosis mice, the protein level of thrombospondin-4 (TSP4) in the aorta, but not in plasma, elevated relatively with atherosclerotic plaque formation. Therefore, we supposed that TSP4 would be a potential biomarker for diagnostic imaging of atherosclerotic progression. Immunoglobulin G (IgG) has been widely used as a basic molecule of imaging probes providing images specific to their target biomolecules, owing to the antigen-antibody reaction. Therefore, we first developed anti-TSP4 monoclonal IgG radiolabeled with ^{99m}Tc (^{99m}Tc-TSP4-mAb). ^{99m}Tc-TSP4-mAb showed higher accumulation in atherosclerotic aortas of apoE$^{-/-}$ mice (atherosclerotic model

Y. Shimizu (✉)
Faculty of Pharmaceutical Sciences, Hokkaido University, Sapporo, Japan

Central Institute of Isotope Science, Hokkaido University, Sapporo, Japan

Graduate School of Medicine, Hokkaido University, Sapporo, Japan
e-mail: yshimizu@pharm.hokudai.ac.jp

H. Hanzawa • T. Sakamoto
Research & Development Group, Hitachi, Ltd., Kokubunji, Tokyo, Japan

Y. Zhao • S. Fukura • S. Zhao
Graduate School of Medicine, Hokkaido University, Sapporo, Japan

K. Nishijima
Central Institute of Isotope Science, Hokkaido University, Sapporo, Japan

Graduate School of Medicine, Hokkaido University, Sapporo, Japan

N. Tamaki
Department of Nuclear Medicine, Graduate School of Medicine, Hokkaido University, Sapporo, Japan

Y. Kuge
Central Institute of Isotope Science, Hokkaido University Department of Integrated Molecular Imaging, Graduate School of Medicine, Hokkaido University, Sapporo, Japan

Y. Kuge et al. (eds.), *Perspectives on Nuclear Medicine for Molecular Diagnosis and Integrated Therapy*, DOI 10.1007/978-4-431-55894-1_11

mice); however, we found that the non-targeted monoclonal IgG radiolabeled with ^{99m}Tc also showed similar distribution in atherosclerotic aortas of apoE$^{-/-}$ mice. IgG has also known to accumulate nonspecifically in the immunological disease such as inflammatory arthritis. However, the accumulation mechanism of IgG has still been unclear in detail. In this chapter, we would like to introduce recent topics on atherosclerotic imaging, focused on our work exploring the accumulation mechanisms of IgG in atherosclerotic lesions, and elucidating the usefulness of radiolabeled IgG images in the diagnosis of atherosclerosis.

Keywords Atherosclerosis • Immunoglobulin G • Polarized macrophage

11.1 Introduction

Rupture of vulnerable plaques and the subsequent thrombogenesis induce ischemic diseases such as cerebral and myocardial infarction [1]. Therefore, it is necessary to detect vulnerable lesions precisely for the diagnosis of such diseases. Various biomolecules are expressed or activated as atherosclerosis progresses. Thus, the detection and imaging of such biomolecules would make possible the determination of the progression of atherosclerosis in detail. In our previous proteomic studies of atherosclerotic model mice [2], the relative thrombospondin-4 (TSP4) levels of atherosclerotic model mice/normal mice in the aorta, but not in plasma, increased with the atherosclerotic plaque formation. TSP4 belongs to the thrombospondin families and has been reported to play some roles such as promotion of proliferation of smooth muscle cells and adhesion and migration of neutrophils [3]. It has also been reported that apoE and TSP4 double knockout mice showed fewer atherosclerotic lesions than the atherosclerosis apoE knockout mice, which suggests that TSP4 has a crucial role in the progression of atherosclerotic lesions [4]. Therefore, we supposed that TSP4 would be a potential biomarker for diagnostic imaging of atherosclerotic progression. Immunoglobulin G (IgG) is widely used particularly for the target-specific imaging of cancer, because it provides images specific to their target biomolecules owing to the antigen-antibody reaction [5]. Thus, we first developed an IgG-based TSP4 targeting SPECT imaging probe (^{99m}Tc-TSP4-mAb). ^{99m}Tc-TSP4-mAb accumulated in the atherosclerotic lesions of apoE$^{-/-}$ mouse aortas. However, ^{99m}Tc-NC-mAb, which was composed of non-targeting IgG, also accumulated highly in the atherosclerotic lesions similar to ^{99m}Tc-TSP4-mAb. IgG itself is known to be delivered to atherosclerotic lesions nonspecifically, but the detailed mechanism of the accumulation is still unknown [6].

In this report, we would like to introduce our above-mentioned work in which we explored the accumulation mechanisms of IgG in atherosclerotic lesions and elucidated the usefulness of radiolabeled IgG imaging in the diagnosis of atherosclerosis.

11.2 Materials and Methods

11.2.1 Materials

All chemicals used in this study were commercially available and of the highest purity. HYNIC-N-hydroxysuccinimide was prepared as previously reported [7]. ^{99m}Tc-pertechnetate was purchased from Nihon Medi-Physics Co., Ltd. (Tokyo, Japan). As a TSP4-targeting monoclonal antibody, we used anti-thrombospondin-4 mouse IgG_{2b} (Clone #276523, R&D Systems, Abingdon, UK). As for the negative control non-targeted mouse IgG, we chose mouse IgG_{2b}, a kappa monoclonal [MG2b-57] isotype control (Abcam, Cambridge, UK) whose immunogen is trinitrophenol + keyhole-limpet hemocyanin (KLH).

11.2.2 Preparation of Radiolabeled IgG

Anti-TSP4 monoclonal IgG (TSP4-mAb) or non-targeting IgG (NC-mAb) was radiolabeled with ^{99m}Tc after derivatization with 6-hydrazinonicotinic acid (HYNIC), as previously reported (Fig. 11.1) [8]. In brief, to HYNIC-N-hydroxysuccinimide (8.25 μg) in *N*,*N*-dimethylformamide (8.25 μl), TSP4-mAb or NC-mAb solution in 0.16 M borate buffer (pH 8.0) (250 μl, 2 mg/ml) was added, and the

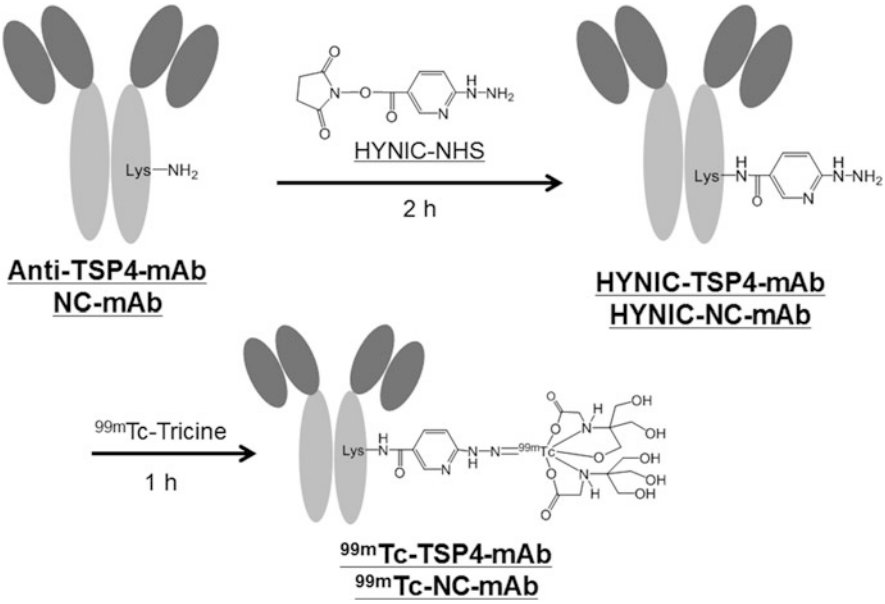

Fig. 11.1 Scheme of ^{99m}Tc-TSP4-mAb or ^{99m}Tc-NC-mAb preparation

mixture was incubated at room temperature for 2 h. The mixture was purified by size-exclusion filtration using a diafiltration membrane (Amicon Ultra 4 [cutoff molecular weight, 30,000]; Millipore Co., Billerica, MA). ^{99m}Tc-(tricine)$_2$(740 MBq/ml, 300 μl) was prepared by the method of Larsen et al. [9]. It was added to the purified solution of HYNIC-TSP4-mAb or NC-mAb solution in 10 mM citrate buffer (pH 5.2) (30 μl, 1 mg/ml), and the mixture was incubated at room temperature for 1 h. The mixture was then purified on a Sephadex G-25 column (PD-10, GE Healthcare, Buckinghamshire, UK) equilibrated with 0.1 M PBS (pH7.4) to obtain ^{99m}Tc-TSP4-mAb or ^{99m}Tc-NC-mAb. The radiochemical purity of ^{99m}Tc-TSP4-mAb or ^{99m}Tc-NC-mAb was measured by size-exclusion filtration of the PD-10 column and size-exclusion high-performance liquid chromatography (HPLC). The stability of ^{99m}Tc-TSP4-mAb or ^{99m}Tc-NC-mAb in plasma was evaluated by the method described below. First, the probes (^{99m}Tc-TSP4-mAb, 27.7 MBq/ml; ^{99m}Tc-NC-mAb, 34.9 MBq/ml; 50 μl) were incubated with the plasma derived from C57BL/6 (male, 30 weeks) for 24 h, and then the mixture was analyzed by size-exclusion filtration of the PD-10 column.

11.2.3 Animal Study

Animal care and all experimental procedures were performed with the approval of the animal care committee of Hokkaido University. Studies were performed using male C57BL/6J apoE$^{-/-}$ mice obtained from the Taconic Gnotobiotic Center (Germantown, NY, USA) and C57BL/6J mice as the wild-type (WT) mice obtained from Charles River Laboratories Japan, Inc. (Yokohama, Japan). The animals were kept in a temperature-controlled facility of the laboratory of animal experiments of Hokkaido University on a 12-h light cycle with free access to food and water. After 5 weeks of age, the apoE$^{-/-}$ mice were maintained on a high-fat diet (21 % fat, 0.15 % cholesterol, without cholate; purchased from Oriental Yeast Ltd., Tokyo, Japan). At 35 weeks of age, the animals ($n = 4$/group) were anesthetized with pentobarbital (0.025 mg/kg body weight, intraperitoneally). ^{99m}Tc-TSP4-mAb (200–592 kBq/mouse) or ^{99m}Tc-NC-mAb (481–962 kBq/mouse) was intravenously injected to each animal. Twenty-four hours after the injection, the animals were euthanized under deep pentobarbital anesthesia, and aortas were fixed by cardiac perfusion with cold 0.1 M phosphate-buffered saline (pH 7.4) followed by a cold fixative [4 % paraformaldehyde, 0.1 M phosphate-buffered solution (pH 7.4)]. Each excised aorta was cut and placed onto glass slides. The dissected aortic root of each mouse was embedded in Tissue-Tek medium (Sakura Finetechnical Co., Ltd., Tokyo, Japan) and frozen in isopentane/dry ice. Serial cross sections of 10-μm (for autoradiographic study) and 5-μm (for immunohistochemistrical analysis) thickness were immediately cut and thaw-mounted on glass slides.

11.2.3.1 Autoradiography (ARG) Study

The excised and cut aortas on glass slides were exposed to phosphor imaging plates (Fuji Imaging Plate BAS-UR, Fujifilm, Tokyo, Japan) for 12 h, together with a set of calibrated standards. The autoradiographic images were acquired using a computerized imaging analysis system (Fuji bio-imaging analyzer FLA7000). The acquired data was analyzed using MultiGauge version 3.2 (Fujifilm).

11.2.4 Histochemical Study

Movat's pentachrome staining of serial aortic root sections was performed [10]. Immunohistochemical staining of the serial sections with a mouse macrophage-specific antibody (Mac-2, clone m3/38, Cedarlane, Ontario, Canada) was performed in accordance with a previously reported immunohistochemical procedure [11]. The TSP4 immunohistochemical staining of the serial sections was performed as shown below. At first, endogenous peroxidase activity was blocked for 10 min with 3 % hydrogen peroxide after rehydration. Slides were then incubated with anti-thrombospondin-4 mouse IgG_{2b} (Clone #276523, R&D Systems) overnight at 4 °C, followed by incubation with a peroxidase-labeled amino acid polymer-conjugated goat anti-mouse F(ab′)2 fragment of IgG (Histofine Mouse Stain kit, Nichirei, Tokyo, Japan) for 30 min at room temperature. The bound antibody complex was then visualized by incubation with 3,3-′-diaminobenzidine tetrahydrochloride. The images of the staining shown above were captured under a microscope (Biozero BZ-8000; Keyence Co., Osaka, Japan).

11.3 Results

11.3.1 Probe Preparation

^{99m}Tc-TSP4-mAb or ^{99m}Tc-NC-mAb was obtained with a radiochemical yield of 17.6 ± 3.8 % or 31.8 ± 6.8 % ($n = 3$) and with the radiochemical purity of 99.5 ± 0.1 % or 99.2 ± 0.5 % ($n = 3$). The stability of ^{99m}Tc-TSP4-mAb or ^{99m}Tc-NC-mAb in the mouse plasma was over 90 % for 24-hour incubation.

11.3.2 In Vivo *Study*

The distributions of ^{99m}Tc-TSP4-mAb in apoE$^{-/-}$ mice and wild-type (WT) mice at 24 h after administration are shown in Table 11.1. The ^{99m}Tc-TSP4-mAb

Table 11.1 Biodistribution of ^{99m}Tc-TSP4-mAb in apoE$^{-/-}$ or wild-type (WT) mice 24 h after administration

	apoE$^{-/-}$	WT
Aorta	5.3 ± 1.1	2.4 ± 0.3
Heart	1.8 ± 0.3	1.5 ± 0.2
Lung	1.7 ± 1.4	1.9 ± 1.6
Liver	5.5 ± 1.8	5.9 ± 1.3
Kidney	2.5 ± 0.2	2.3 ± 0.3
Stomach	1.8 ± 0.5	1.1 ± 0.2
Small intestine	1.3 ± 0.2	1.5 ± 0.2
Large intestine	3.8 ± 1.9	2.5 ± 0.3
Pancreas	0.8 ± 0.2	0.7 ± 0.1
Spleen	7.5 ± 1.2	6.7 ± 0.8
Brain	0.1 ± 0.1	0.1 ± 0.0
Muscle	0.5 ± 0.2	0.6 ± 0.1
Blood	17.2 ± 2.1	17.2 ± 1.5

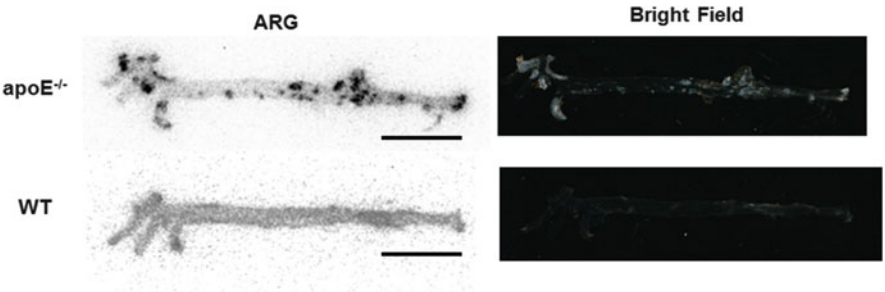

Fig. 11.2 ARG images (*left*) and bright field images (*right*) of the excised aortas of apoE$^{-/-}$ mouse (*upper*) and of wild-type (WT) mouse (*lower*) 24 h after administration of ^{99m}Tc-TSP-mAb

accumulation levels in the aortas of apoE$^{-/-}$ mice were significantly higher than those in WT mice (5.3 ± 1.1 vs. 2.4 ± 0.3 %ID/g, $p < 0.05$), whereas the radioactivities in other organs were not significantly different between apoE$^{-/-}$ mice and wild mice. On the other hand, the ^{99m}Tc-NC-mAb accumulation levels in the aortas of apoE$^{-/-}$ mice were also significantly higher than those of WT mice (5.1 ± 1.4 vs. 2.8 ± 0.5 %ID/g, $p < 0.05$), whereas the radioactivities in other organs were not different between apoE$^{-/-}$ mice and wild-type mice.

The ARG images of the apoE$^{-/-}$ aortas injected with ^{99m}Tc-TSP4-mAb showed heterogeneous distribution of the radioactivity where the plaque formation was observed in the bright field (Fig. 11.2). The radioactive distribution in the aortic roots of apoE$^{-/-}$ mice injected with ^{99m}Tc-TSP4-mAb measured by ARG was inside of the atherosclerotic plaque lesions and coincided with the Mac-2-positive areas (Fig. 11.3). These results suggest that ^{99m}Tc-TSP4-mAb accumulated in the macrophage-infiltrated area of the plaque lesions.

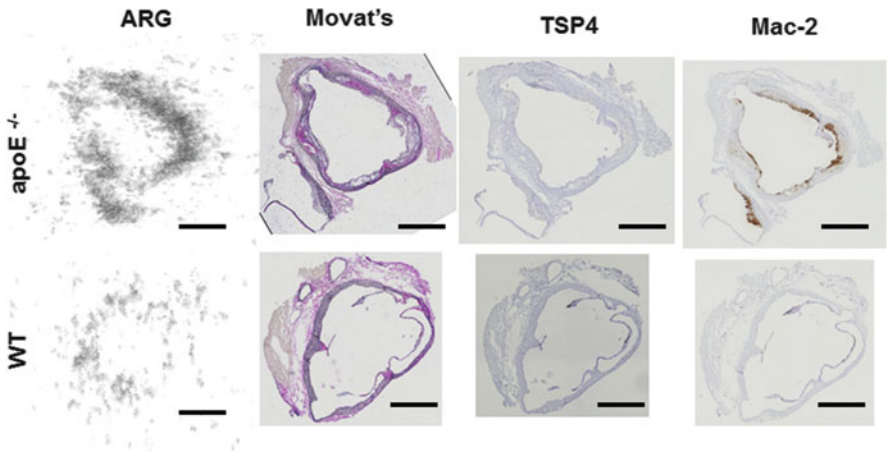

Fig. 11.3 ARG images, Movat's pentachrome staining, TSP4 immunohistochemical staining, and Mac-2 immunohistochemical staining of the aortic roots of apoE$^{-/-}$ mouse (*upper*) and wild-type (WT) (*lower*) mouse 24 h after administration of ^{99m}Tc-TSP4-mAb

11.3.3 Discussion

In this study, we observed that ^{99m}Tc-TSP4-mAb accumulated in the atherosclerotic lesions of apoE$^{-/-}$ mouse aortas. However, ^{99m}Tc-NC-mAb, which was composed of non-targeting IgG, also accumulated highly in the atherosclerotic lesions similar to ^{99m}Tc-TSP4-mAb (Fig. 11.2). Moreover, the ^{99m}Tc-TSP4-mAb accumulation area coincided with the Mac-2-positive areas in the plaques in aortic root (Fig. 11.3), which suggests that IgG itself was delivered and accumulated in atherosclerotic lesions, especially macrophage infiltration areas.

Previously, various types of polarized macrophage were identified and reported [12]. Among the polarized macrophages, pro-inflammatory M1-polarized macrophages were reported to be abundant in lipids and to localize in areas that are distinct from those in which anti-inflammatory M2-polarized macrophages (which are also called alternatively activated macrophages) localize in human plaques [13]. Although the origin of M1 and polarized macrophages and how polarized macrophages are involved in the progression of atherosclerotic plaques are still being unclarified, polarized macrophages would have a critical role in the development of atherosclerotic plaques [14]. Therefore, we examined the correlation of the macrophages, especially polarized macrophages, with IgG accumulation. In our preliminary in vitro study, M1-polarized macrophages showed a higher uptake of ^{99m}Tc-NC-mAb than M2-polarized and non-polarized M0 macrophages [15]. To clarify the mechanism of ^{99m}Tc-NC-mAb accumulation in M1-polarized macrophages, we next focus on the expression levels of Fcγ receptors. Fcγ receptors recognize the Fc region of IgG and play a role in the activation of immune systems [16]. Furthermore, it has been reported that deficiency of Fcγ receptors induces

protection against atherosclerosis in apoE$^{-/-}$ mice [17]. Indeed, the expression level of some subtypes of Fcγ receptors was higher in M1-polarized macrophages than those in M2-polarized or non-polarized M0 macrophages in our unreported in vitro study. We also performed a cellular uptake study under the Fcγ receptor's inhibition and found that the accumulation of ^{99m}Tc-NC-mAb in M1-polarized macrophages was significantly suppressed by the pretreatment with an anti-Fcγ receptor antibody. These findings suggest that IgG itself is accumulated in M1-polarized macrophages via Fcγ receptors in the atherosclerotic plaques.

During the course of atherosclerotic progression, various biomolecules are expressed or activated. Thus, various PET/SPECT imaging probes targeting biomolecules related to the progression of atherosclerosis have been developed [18]. Among them, some probes are developed with based on monoclonal IgG and have been evaluated in animal models such as mouse and rabbit [19, 20]. In those studies, xenogeneic antibodies were used, whose nonspecific accumulation in atherosclerotic lesions was not taken into consideration. However, considering that the probes will be used clinically, the IgG used as a basic component of probes should be humanized, and it would be necessary to note its nonspecific accumulation as we have seen in this study.

Radiolabeled IgG has been widely applied to the diagnosis of inflammatory diseases such as rheumatoid arthritis and infections, although the mechanism of its accumulation is still unclarified [21]. Our preliminary study is the first to show that pro-inflammatory M1-polarized macrophages contribute to the accumulation of radiolabeled IgG, which is in agreement with the conventional use of such IgG as mentioned above.

In the nuclear imaging for diagnosis of atherosclerosis, 18-fluoro-deoxyglucose (^{18}F-FDG) has been widely used [22]. ^{18}F-FDG is reported to accumulate in macrophages, particularly M1-polarized macrophages in atherosclerotic lesions [23], which is similar to radiolabeled IgG behavior. Therefore, radiolabeled IgG would provide information similarly to ^{18}F-FDG in the diagnosis of atherosclerosis.

In this study, we found that IgG itself can be potentially used for the visualization of atherosclerotic plaques, especially atherosclerotic lesions in active inflammation independent of its target biomolecules. However, we also observed the high retention of radioactivities in blood 24 h after administration of ^{99m}Tc-TSP4-mAb (apoE$^{-/-}$, 17.2 ± 2.1 %ID/g; WT, 17.2 ± 1.5 %ID/g), which were about three times higher than those in aortas. This may be because that IgG has a high molecular weight (about 150 kDa), which leads to a low rate of clearance from blood. To overcome this problem, the molecular weight of IgG should be decreased with its affinity to Fcγ receptors maintained. That is, an Fc fragment (about 50 kDa) obtained from IgG would be a suitable basic compound for atherosclerotic imaging. We are now developing an Fc fragment-based probe and evaluating to determine whether this probe can be used to visualize the inflammatory active areas of atherosclerotic lesions.

Acknowledgments This study was supported in part by MEXT KAKENHI (Grant Numbers: 24890003 and 26860961) and the Creation of Innovation Centers for Advanced Interdisciplinary Research Areas Program, Ministry of Education, Culture, Sports, Science and Technology, Japan.

References

1. Ruberg FL, Leopold JA, Loscalzo J. Atherothrombosis: plaque instability and thrombogenesis. Prog Cardiovasc Dis. 2002;44:381–94.
2. Hanzawa H, Sakamoto T, Kaneko A, Manri N, Zhao Y, et al. Combined plasma and tissue proteomic study of atherogenic model mouse: approach to elucidate molecular determinants in atherosclerosis development. J Proteome Res. 2015;14:4257–69.
3. Stenina OI, Desai SY, Krukovets I, Kight K, Janigro D, Topol EJ, et al. Thrombospondin-4 and its variants: expression and differential effects on endothelial cells. Circulation. 2003;108:1514–9.
4. Frolova EG, Pluskota E, Krukovets I, Burke T, Drumm C, Smith JD, et al. Thrombospondin-4 regulates vascular inflammation and atherogenesis. Circ Res. 2010;107:1313–25.
5. Larson SM. Radiolabeled monoclonal anti-tumor antibodies in diagnosis and therapy. J Nucl Med. 1985;26:538–45.
6. Fischman AJ, Rubin RH, Khaw BA, Kramer PB, Wilkinson R, Ahmad M, et al. Radionuclide imaging of experimental atherosclerosis with nonspecific polyclonal immunoglobulin G. J Nucl Med. 1989;30:1095–100.
7. Abrams MJ, Juweid M, TenKate CI, Schwartz DA, Hauser MM, Gaul FE, et al. Technetium-99m-human polyclonal IgG radiolabeled via the hydrazino nicotinamide derivative for imaging focal sites of infection in rats. J Nucl Med. 1990;31:2022–8.
8. Ono M, Arano Y, Mukai T, Uehara T, Fujioka Y, Ogawa K, et al. Plasma protein binding of (99m)Tc-labeled hydrazino nicotinamide derivatized polypeptides and peptides. Nucl Med Biol. 2001;28:155–64.
9. Larsen SK, Solomon HF, Caldwell G, Abrams MJ. [99mTc]tricine: a useful precursor complex for the radiolabeling of hydrazinonicotinate protein conjugates. Bioconjug Chem. 1995;6:635–8.
10. Vucic E, Dickson SD, Calcagno C, Rudd JH, Moshier E, Hayashi K, et al. Pioglitazone modulates vascular inflammation in atherosclerotic rabbits noninvasive assessment with FDG-PET-CT and dynamic contrast-enhanced MR imaging. JACC Cardiovasc Imaging. 2011;4:1100–9.
11. Zhao Y, Kuge Y, Zhao S, Morita K, Inubushi M, Strauss HW, et al. Comparison of 99mTc-annexin A5 with 18F-FDG for the detection of atherosclerosis in ApoE−/− mice. Eur J Nucl Med Mol Imaging. 2007;34:1747–55.
12. Mantovani A, Sica A, Sozzani S, Allavena P, Vecchi A, Locati M. The chemokine system in diverse forms of macrophage activation and polarization. Trends Immunol. 2004;25:677–86.

13. Chinetti-Gbaguidi G, Baron M, Bouhlel MA, Vanhoutte J, Copin C, Sebti Y, et al. Human atherosclerotic plaque alternative macrophages display low cholesterol handling but high phagocytosis because of distinct activities of the PPARgamma and LXRalpha pathways. Circ Res. 2011;108:985–95.
14. Moore KJ, Sheedy FJ, Fisher EA. Macrophages in atherosclerosis: a dynamic balance. Nat Rev Immunol. 2013;13:709–21.
15. Shimizu Y, Hanzawa H, Zhao Y, Fukura S, Nishijima K, Sakamoto T, et al. Accumulation mechanism of non-targeted immunoglobulin G in atherosclerotic lesions. J Nucl Med. 2015;56 Suppl 3:462.
16. Ravetch JV, Bolland S. IgG Fc receptors. Annu Rev Immunol. 2001;19:275–90.
17. Hernandez-Vargas P, Ortiz-Munoz G, Lopez-Franco O, Suzuki Y, Gallego-Delgado J, Sanjuan G, et al. Fcgamma receptor deficiency confers protection against atherosclerosis in apolipoprotein E knockout mice. Circ Res. 2006;99:1188–96.
18. Temma T, Saji H. Radiolabeled probes for imaging of atherosclerotic plaques. Am J Nucl Med Mol Imaging. 2012;2:432–47.
19. Nakamura I, Hasegawa K, Wada Y, Hirase T, Node K, Watanabe Y. Detection of early stage atherosclerotic plaques using PET and CT fusion imaging targeting P-selectin in low density lipoprotein receptor-deficient mice. Biochem Biophys Res Commun. 2013;433:47–51.
20. Temma T, Ogawa Y, Kuge Y, Ishino S, Takai N, Nishigori K, et al. Tissue factor detection for selectively discriminating unstable plaques in an atherosclerotic rabbit model. J Nucl Med. 2010;51:1979–86.
21. Signore A, Prasad V, Malviya G. Monoclonal antibodies for diagnosis and therapy decision making in inflammation/infection. Foreword. Q J Nucl Med Mol Imaging. 2010;54:571–3.
22. Rudd JH, Warburton EA, Fryer TD, Jones HA, Clark JC, Antoun N, et al. Imaging atherosclerotic plaque inflammation with [18F]-fluorodeoxyglucose positron emission tomography. Circulation. 2002;105:2708–11.
23. Satomi T, Ogawa M, Mori I, Ishino S, Kubo K, Magata Y, et al. Comparison of contrast agents for atherosclerosis imaging using cultured macrophages: FDG versus ultrasmall superparamagnetic iron oxide. J Nucl Med. 2013;54:999–1004.